Curley Allison Nicole (Orcid ID: 0000-0002-5885-4733)

Biologically driven isotopic fractionations in bivalves: from palaeoenvironmental problem to palaeophysiological proxy

Allison N. Curley[1,*], Sierra V. Petersen[1], Stewart M. Edie[2] and Weifu Guo[3]

[1]*Department of Earth and Environmental Sciences, University of Michigan, Ann Arbor, MI 48109, USA*

[2]*Department of Paleobiology, National Museum of Natural History, Smithsonian Institution, Washington, DC 20013, USA*

[3]*Department of Geology and Geophysics, Woods Hole Oceanographic Institution, Woods Hole, MA 02543, USA*

[*]Author for correspondence (E-mail: ancurley@umich.edu; Tel.: +1 908 783 0491).

ABSTRACT

Traditional bulk stable isotope ($\delta^{18}O$ and $\delta^{13}C$) and clumped isotope (Δ_{47}) records from bivalve shells provide invaluable histories of Earth's local and global climate change. However, biologically driven isotopic fractionations (BioDIFs) can overprint primary environmental signals in the shell. Here, we explore how conventional measurements of $\delta^{18}O$, $\delta^{13}C$, and Δ_{47} in bivalve shells can be re-interpreted to investigate these physiological processes deliberately. Using intrashell Δ_{47} and $\delta^{18}O$ alignment as a proxy for equilibrium state, we separately examine fractionations and/or disequilibrium occurring in the two major stages of the biomineralization process: the secretion of the extrapallial fluid (EPF) and the

This is the author manuscript accepted for publication and has undergone full peer review but has not been through the copyediting, typesetting, pagination and proofreading process, which may lead to differences between this version and the Version of Record. Please cite this article as doi: 10.1111/brv.12940

This article is protected by copyright. All rights reserved.

Author Manuscript

Author Manuscript

precipitation of shell material from the EPF. We measured $\delta^{18}O$, $\delta^{13}C$, and Δ_{47} in fossil shells representing five genera (*Lahillia*, *Dozyia*, *Eselaevitrigonia*, *Nordenskjoldia*, and *Cucullaea*) from the Maastrichtian age [66–69 million years ago (Ma)] López de Bertodano Formation on Seymour Island, Antarctica. Material was sampled from both the outer and inner shell layers (OSL and ISL, respectively), which precipitate from separate EPF reservoirs. We find consistent $\delta^{18}O$ values across the five taxa, indicating that the composition of the OSL can be a reliable palaeoclimate proxy. However, relative to the OSL baseline, ISLs of all taxa show BioDIFs in one or more isotopic parameters. We discuss/hypothesize potential origins of these BioDIFs by synthesizing isotope systematics with the physiological processes underlying shell biomineralization. We propose a generalized analytical and interpretive framework that maximizes the amount of palaeoenvironmental and palaeobiological information that can be derived from the isotopic composition of fossil shell material, even in the presence of previously confounding 'vital effects'. Applying this framework in deep time can expand the utility of $\delta^{18}O$, $\delta^{13}C$, and Δ_{47} measurements from proxies of past environments to proxies for certain biomineralization strategies across space, time, and phylogeny among Bivalvia and other calcifying organisms.

CONTENTS

I. Introduction

II. Anatomy of bivalve biomineralization

III. Isotopic proxies applied in biomineralization studies

(1) Bulk oxygen and carbon isotopes

(2) Clumped isotopes

IV. Isotopic equilibrium in dissolved inorganic carbonate species

V. Timing of isotopic fractionation during key steps of biomineralization

(1) EPF formation

(2) Shell precipitation

VI. Example application: Seymour Island, Antarctica (69–66 Ma)

(1) Materials and methods

(2) OSL carbonate records the external environment

(3) Species-specific BioDIFs detected in ISL

(*a*) Isotopic trends in ISL values

(*b*) Identifying types of BioDIFs

(4) Potential drivers of BioDIFs

(*a*) Enrichment in Δ_{47} with depletion in $\delta^{18}O$ and $\delta^{13}C$

(*b*) Depletion in Δ_{47} with enrichment in $\delta^{18}O$ and $\delta^{13}C$

(5) Implications for palaeotemperature reconstructions at Seymour Island

VII. A workflow for interpreting BioDIFs

VIII. Implications and future prospects

IX. Conclusions

X. Acknowledgements

XI. References

XII. Supporting information

I. INTRODUCTION

Clumped isotopes (Δ_{47} and more recently Δ_{48}) and bulk stable isotopes ($\delta^{18}O$ and $\delta^{13}C$) in biogenic carbonates are commonly used to study temperature, salinity, and carbon cycling in the geological past (Eiler, 2007). The relationship between the isotopic composition and temperature of growth water and the isotopic composition of precipitated calcium carbonate ($CaCO_3$) has been calibrated in modern contexts using synthetic and/or

Author Manuscript

Author Manuscript

naturally occurring carbonates precipitated in equilibrium (Ghosh *et al.*, 2006; Kelson *et al.*, 2017; Petersen *et al.*, 2019; Daëron *et al.*, 2019; Anderson *et al.*, 2021; Bernasconi *et al.*, 2021). The isotopic composition of mollusc shells made of $CaCO_3$ has long been used as a recorder of environmental temperature and chemistry (e.g. Epstein *et al.*, 1951). Thanks to their wide distribution and preservation in space and time (Moss, Ivany & Jones, 2021), fossilized mollusc shells are especially useful for deep-time palaeoclimate reconstructions that are beyond the reach of many other palaeoclimate proxy methods. Bivalve shells in particular have been shown to record environmental chemistry accurately (e.g. Schöne & Surge, 2012; Henkes *et al*., 2013; Caldarescu *et al*., 2021).

Unfortunately, cryptic biological processes can cause isotopic and elemental fractionations (i.e. preferential partitioning of certain isotopes or elements) that affect the geochemical relationships between shell carbonate and ambient water (McConnaughey, 1989). These result in a geochemical signature in the shell that differs from that expected based on the known equilibrium relationships, making it difficult or impossible to infer environmental information from the isotopic composition of the shell. Such fractionations have historically been collectively termed 'vital effects', referencing their origin in poorly understood vital processes. Myriad isotopic effects across widely diverse taxa are placed under this catch-all term because, ultimately, any divergence from baseline abiogenic behaviour renders the isotopic data uninterpretable in a palaeoenvironmental context without additional empirical calibrations (e.g. Fenger *et al*., 2007; Henkes *et al*., 2013; Parker *et al*., 2017). Here we argue that this generalized terminology masks potentially meaningful and interpretable differences in isotopic behaviour among taxa, hindering or discouraging investigations into this aspect of the palaeophysiological record. While these fractionations are not interpretable within our usual palaeoclimatological framework, a new palaeophysiological framework can be developed using the same first principles of isotope

Author Manuscript

geochemistry. In light of the growing approachability of isotopic behaviour within the biological system, we suggest a move away from the 'black box' terminology of 'vital effects' in favour of the more precise 'biologically driven isotopic fractionations (BioDIFs)' to describe specific, quantifiable fractionations of determinable physiological origins.

Although necessarily avoided in palaeoenvironmental studies, if understood mechanistically, BioDIFs are a potentially informative (if presently understudied) component of the fossil record. The physiology of biomineralization in living bivalves has been studied for decades (Yarra, Blaxter & Clark, 2021) using controlled *in situ* observations and experimentation on live animals. However, it remains difficult to extend these insights to the geological past because fossil material is limited to mineralized hard parts. A few studies have linked BioDIFs in the shell geochemistry of modern taxa to possible physiological drivers (e.g. Weiner & Dove, 2003; McConnaughey & Gillikin, 2008; Schöne, 2008; Ezard, Edgar & Hull, 2015), but a generalizable framework for relating those observations on modern taxa to the fossil record remains underdeveloped. Technical advances in clumped isotope palaeothermometry (e.g. Guo & Zhou, 2019; Guo, 2020; Bajnai *et al*., 2020), namely the coupling of Δ_{47} measurements to $\delta^{18}O$ and Δ_{48} measurements as a disequilibrium proxy, can now distinguish BioDIFs occurring at different stages of the biomineralization process using shell material alone. This is a new step forward in unravelling what physiological signals may be archived in fossil shells. Independently of mechanistic interpretations, systematic sampling of BioDIFs across many taxa and environments through time would allow us to observe the variability of these traits within class Bivalvia and investigate their relationships to other aspects of organismal physiology, phylogeny, and environment. Overall, this presents a new avenue for expanding our knowledge of bivalve biodiversity through geological time.

Author Manuscript

Here, we suggest that by measuring the composition of fossil shells using novel and established isotopic proxies, 'vital effects' can in some cases be reframed as quantifiable and interpretable BioDIFs – providing a new perspective on organismal palaeophysiology. Uniting the power of these updated methodologies with the temporal scope of the fossil record can provide new perspectives on the metabolic demands of calcification, how biomineralization pathways have evolved within major groups of biomineralizing organisms, and whether differences in these pathways confer resilience during adverse environmental changes.

II. ANATOMY OF BIVALVE BIOMINERALIZATION

Bivalves tightly regulate their shell formation (Ponder, Lindberg & Ponder, 2020), which is a process that often changes over an individual's lifespan [e.g. ontogenetic changes in growth rate (Lorrain *et al*., 2004; Carré *et al*., 2006); partitioning of carbonate volume among shell sectors (Nishida & Sasaki, 2018); and changing isotopic/elemental composition after reaching sexual maturity (Jones, Williams & Romanek, 1986; Romanek *et al*., 1987)]. Shell precipitation is directed by the shell-facing mantle epithelial cells, which synthesise proteins and other biomacromolecules that regulate $CaCO_3$ nucleation (Rodríguez-Navarro *et al.*, 2016; Wolf *et al.*, 2016). The first $CaCO_3$ formed is likely in a transient amorphous phase (amorphous calcium carbonate; ACC) (e.g. Weiss *et al.*, 2002; Addadi *et al.*, 2006; Jacob *et al.*, 2011; Gal *et al.*, 2014; Gal, Weiner & Addadi, 2015; Hovden *et al.*, 2015), which originates intracellularly in the mantle epithelium and may or may not be dissolved and reformed once exocytosed to the extrapallial fluid (EPF) (Rodríguez-Navarro *et al.*, 2016; Wolf *et al.*, 2016). The EPF, known as the calcifying fluid of bivalves, is housed in the narrow space (<100 nm) between the shell and the mantle epithelium (Nakahara & Bevelander, 1971; Nakahara, 1991; Checa *et al*., 2014) (Fig. 1). Measurements of EPF (e.g.

Author Manuscript

Crenshaw, 1972; Moura, Machado & Coimbra, 2003) indicate that it concentrates precursors to $CaCO_3$, containing dissolved inorganic carbonate (DIC) species (CO_2, HCO_3^-, CO_3^{2-}) and calcium (and other divalent cations) both in ionic form (Ca^{2+}) and within organic complexes. The EPF also contains many proteins, lipids, and other organic compounds produced by the mantle epithelial cells (e.g. Moura *et al.*, 2000; Marin & Luquet, 2004; Addadi *et al.*, 2006; Marin *et al.*, 2007; Clark *et al.*, 2020; Yarra *et al.*, 2021).

In most bivalves (with some scallops and oysters being notable exceptions), the mantle attaches to the shell along a continuous front, often observed as a slight impression on the inner shell surface termed the 'pallial line'. This line is typically inset from the ventral margin and marks the division of the EPF into two adjacent chambers (Fig. 1). Ventral to the pallial line is the outer EPF (oEPF), which is bounded by the mantle edge, the mantle attachment at the pallial line, the shell, and the periostracum (an organic cuticle-like layer; Ponder *et al.*, 2020) (Fig. 1). The oEPF and its associated mantle epithelium provide the precursor molecules for formation of the outer shell layer (OSL) and the middle shell layer (when present) (Weiner & Dove, 2003; Addadi *et al.*, 2006; Marin *et al.*, 2007; Schöne & Surge, 2012; Gannon *et al.*, 2017). Dorsal to the pallial line is the inner EPF (iEPF), which is bounded by the dorsal mantle, the mantle attachment at the pallial line, and the shell (Fig. 1). The iEPF and its associated mantle epithelium provide the precursor molecules for formation of the inner shell layer (ISL) (Schöne & Surge, 2012).

III. ISOTOPIC PROXIES APPLIED IN BIOMINERALIZATION STUDIES

The isotopic composition of the solid shell contains information about the original inhabited environment and the processes of shell formation.

(1) Bulk oxygen and carbon isotopes

Author Manuscript

The $\delta^{18}O$ value of any carbonate ($\delta^{18}O_{carb}$, the ratio of $^{18}O/^{16}O$ relative to a standard) is a function of both ambient water temperature and the $\delta^{18}O$ of the fluid from which it precipitates. Synthetic carbonate precipitation experiments used to calibrate this oxygen isotope palaeothermometer empirically derive relationships between $\delta^{18}O_{carb}$, experimentally controlled temperature, and experimentally controlled growth water ($\delta^{18}O_{water}$) (e.g. Kim & O'Neil, 1997; Zhou & Zheng, 2006; Kim *et al.*, 2007). This relationship can be linearized to the form $T = A + B(\delta^{18}O_{carb} + \delta^{18}O_{water})$.

In bivalve shells, $\delta^{18}O_{carb}$ can be used to investigate changes in environmental temperature and local water chemistry. However, unlike a synthetic carbonate precipitating directly from the surrounding water, $\delta^{18}O_{carb}$ of a bivalve shell is precipitated from the contents of the EPF, which has a composition ($\delta^{18}O_{EPF}$) that may or may not differ from the primary environmental signal ($\delta^{18}O_{water}$) (see Section V.1). Given the interdependency between the measured $\delta^{18}O_{carb}$ and two unknown values ($\delta^{18}O_{EPF}$ and temperature), external information or reasonable assumptions about one of the two unknowns is necessary to calculate a value for the remaining variable. Calculating $\delta^{18}O_{EPF}$ is of particular interest when seeking to determine if $\delta^{18}O_{EPF}$ was biologically fractionated from $\delta^{18}O_{water}$, so a temperature value must be supplied from an external source, such as clumped isotope measurements (see Section III.2).

The $\delta^{13}C$ value of shell carbonate ($\delta^{13}C_{carb}$, the ratio of $^{13}C/^{12}C$ relative to a standard) reflects a mixture of external DIC (eDIC) from the surrounding environment and metabolic DIC (mDIC) produced within the soft tissues. The mDIC typically has more negative $\delta^{13}C$ values than eDIC (e.g. Gillikin *et al.*, 2007; McConnaughey & Gillikin, 2008) and is generally thought to contribute carbon to less than 10% of shell carbonate (e.g. McConnaughey *et al.*, 1997), although higher fractions have sometimes been reported (e.g. Gillikin *et al*., 2007). Because of the variability in composition and mixing proportions of

these DIC pools, which are often poorly understood across species, $\delta^{13}C_{carb}$ values of fossil bivalve shells are not typically used to reconstruct $\delta^{13}C_{eDIC}$ (McConnaughey & Gillikin, 2008). Still, $\delta^{13}C_{carb}$ can be useful for tracking larger-scale changes in the carbon cycle and primary productivity (see review by Mackensen and Schmiedl, 2019).

(2) Clumped isotopes

Clumped isotope analysis overcomes some of the limitations of oxygen isotope palaeothermometry (Eiler, 2007), and can also serve as an indicator of isotopic equilibrium *versus* disequilibrium precipitation. Under thermodynamic equilibrium, the temperature of ambient water controls the bonding frequency of heavy O and C isotopes in $CaCO_3$ (Ghosh *et al.*, 2006). The relationship between formation temperature and Δ_{47} (the excess abundance of mass-47 CO_2 molecules derived from $CaCO_3$ relative to their expected stochastic abundance, independent of bulk isotopic composition) has been well calibrated using synthetic carbonates, and most biogenic carbonates follow the same relationships (e.g. Ghosh *et al.*, 2006; Kelson *et al.*, 2017; Petersen *et al.*, 2019; Anderson *et al.*, 2021; Bernasconi *et al.*, 2021). This relationship generally has the form $\Delta_{47} = A \times 10^6 \times T^{-2} + B$. Simultaneous analysis of $\delta^{18}O_{carb}$ and Δ_{47} (which provides a direct temperature measurement) circumvents the need to assume environmental temperature to calculate $\delta^{18}O_{EPF}$.

Improvements in analytical precision have also made it possible to analyse Δ_{48}, which quantifies CO_2 with a mass of 48 atomic mass units (another multiply substituted isotopologue whose occurrence is also temperature dependent and independent of bulk isotopic composition under equilibrium conditions) (Guo, 2020; Bajnai *et al.*, 2020). Because under thermodynamic equilibrium Δ_{47}, Δ_{48}, and $\delta^{18}O_{carb}$ all relate to temperature in predictable ways, deviations from the expected values indicate isotopic disequilibrium in the EPF at the time of precipitation (Guo & Zhou, 2019; Guo, 2020). Pairing any two of these

Author Manuscript

Author Manuscript

temperature-dependent isotopic proxies can confirm whether a shell precipitated under equilibrium or disequilibrium conditions, and can also characterize the mechanism of fractionation (Guo & Zhou, 2019; Guo, 2020; Bajnai *et al.*, 2020). Enrichment in Δ_{47} combined with depletions in $\delta^{18}O_{carb}$ and/or Δ_{48} is consistent with CO_2 absorption; depletion in Δ_{47} combined with enrichment in $\delta^{18}O_{carb}$ and/or Δ_{48} implicate CO_2 degassing (Guo, 2020; Bajnai *et al.*, 2020) (see Section VI.4). A benefit of pairing Δ_{47} and Δ_{48} specifically is that it is possible to reconstruct the true formation temperature even when the Δ_{47} and Δ_{48} values are offset from the equilibrium line, especially when a modelled linear slope can be applied (Guo, 2020; Bajnai *et al.*, 2020). Using $\delta^{18}O_{carb}$ to identify disequilibrium and reconstruct temperature in this way requires additional assumption or measurements of $\delta^{18}O_{EPF}$ to define the temperature relationship with either Δ_{47} or Δ_{48}.

IV. ISOTOPIC EQUILIBRIUM IN DISSOLVED INORGANIC CARBONATE SPECIES

DIC species (CO_2, HCO_3^-, CO_3^{2-}) exist in a pH-dependent chemical equilibrium (i.e. the relative abundance of each chemical species is maintained at a known steady state at a given pH). This equilibrium is maintained by the ability to transform spontaneously from one species to another by reaction with hydroxide ion (hydroxylation/dehydroxylation; reaction 1), reaction with water (hydration/dehydration; reaction 2), or by gaining/losing a proton (protonation/ deprotonation; reaction 3).

$$CO_2 + OH^- \leftrightarrow HCO_3^- \quad (1)$$

$$CO_2 + H_2O \leftrightarrow HCO_3^- + H^+ \quad (2)$$

$$HCO_3^- \leftrightarrow CO_3^{2-} + H^+ \quad (3)$$

These bidirectional reactions occur continuously and simultaneously in solution. Transformations between chemical species can be directly accompanied by certain kinetic isotope

fractionations. Some geochemical processes (e.g. CO_2 degassing) involve multiple reactions that can amount to a particular net kinetic isotope effect when conditions are favourable (e.g. the kinetic signature of CO_2 degassing is higher $\delta^{18}O$, $\delta^{13}C$ and Δ_{48} values and lower Δ_{47} values in the residual HCO_3^- and CO_3^{2-}) (Guo & Zhou, 2019; Guo, 2020). Two conditions must be met in a closed system to prevent a kinetic fractionation signature from being recorded in the precipitated $CaCO_3$: (1) the species in these reversible reactions must be able to interconvert freely and exchange isotopes in both directions; and (2) sufficient time must be given for the aforementioned isotope exchange to occur. If open or partially open system behaviour is allowed, it may also be possible to 'dilute' the fractionation signature through mixing with isotopically equilibrated eDIC. The limited DIC pool involved in shell formation, existing in the EPF and mantle epithelium, may be especially susceptible to accumulating an overall kinetic isotope signature due to the limited opportunity for mixing (either laterally within the EPF or with eDIC), especially in the iEPF.

Deprotonation reactions (e.g. reaction 3) reestablish chemical equilibrium between HCO_3^- and CO_3^{2-} in seconds, isotopically equilibrating these species similarly quickly (Guo & Zhou, 2019; Guo, 2020). These reactions are therefore not primarily responsible for creating the isotopic disequilibrium signatures recorded in the shell material and it can be assumed that CO_3^{2-} and HCO_3^- are always in isotopic equilibrium with each other. By contrast, the (de)hydration and (de)hydroxylation reactions that convert between CO_2 and HCO_3^- require minutes to hours to establish isotopic equilibrium, so the net kinetic signature is preserved for a longer time with a greater chance that $CaCO_3$ will precipitate from an isotopically anomalous HCO_3^- ion (or CO_3^{2-} equilibrated with an isotopically anomalous HCO_3^- ion) (Guo & Zhou, 2019; Guo, 2020). Re-equilibration occurs when HCO_3^- or CO_2 can freely interconvert and exchange isotopes, but certain conditions (e.g. fluxes of reactant or product ions, fluid pH) can push these reactions out of balance and inequitably favour production of either HCO_3^- or CO_2. When this is the case, certain

Author Manuscript

disequilibrium signatures may be created and sustained in the HCO_3^- pool long enough to be recorded in the precipitated shell.

V. TIMING OF ISOTOPIC FRACTIONATION DURING KEY STEPS OF BIOMINERALIZATION

Bivalve shell formation occurs in two major stages: the EPF formation phase, which produces calcifying fluid and concentrates precursor ions in the EPF, and the precipitation phase, wherein the constituents of the EPF are used to construct a solid $CaCO_3$ shell (see Wilbur & Saleuddin, 1983). BioDIFs, the offset in isotopic composition of the final shell material relative to expectations given environmental temperature and ambient water composition, can be produced in either or both of these steps.

(1) EPF formation

Precursor ions to $CaCO_3$ can be incorporated into the EPF *via* one of two pathways: (1) mixing the EPF with precursor ions constituting eDIC (Fig. 1, arrow 1a); or (2) transport of precursor ions constituting mDIC into and across the mantle epithelium (Fig. 1, arrow 1b). The bulk isotopic composition of eDIC reflects ambient water ($\delta^{18}O_{water}$, $\delta^{13}C_{eDIC}$) and its carbonate species are likely in both chemical and isotopic equilibrium due to their derivation from a large reservoir with a long timescale for equilibrium exchange. The mDIC derives from vital processes such as respiration, metabolism of food, creation/maintenance of body tissues, reproduction, and many more metabolic demands, each of which can cause isotopic fractionations and disequilibrium such that $\delta^{13}C_{mDIC}$ can differ from $\delta^{13}C_{eDIC}$ (e.g. Elliot *et al*., 2003; Lorrain *et al*., 2004; Gillikin *et al*., 2007). Isotopic fractionations could also occur during transport across the mantle epithelium into the EPF, although this is difficult to observe directly in isolation.

Author Manuscript

Author Manuscript

Because the OSL of bivalve shells has consistently been shown to record environmental temperature and $\delta^{18}O_{water}$ accurately, the oEPF evidently tends to maintain isotopic equilibrium with ambient water. Due to its ventral positioning, it may be more likely to mix with ambient water, perhaps passively or when the mantle lobes are deeply retracted within the inner cavity (e.g. Carriker, 1992; McConnaughey & Gillikin, 2008), or it may remain isolated but not experience isotopic fractionations for reasons yet unknown.

If mixing indeed occurs, the isotopic composition of the oEPF ($\delta^{18}O_{oEPF}$ and $\delta^{13}C_{oEPF}$) reflects a mixture of eDIC and mDIC (Shanahan *et al.*, 2005; Gillikin *et al.*, 2007; McConnaughey & Gillikin, 2008), with eDIC potentially constituting the majority of DIC in the oEPF. The iEPF is comparatively less likely to mix with ambient water given its physical isolation from the environment (Carriker, 1992), making metabolism and transport across the mantle (Fig. 1, arrow 1b) the predominant pathway for delivery of precursor ions to the iEPF.

Here we treat all these processes as a single step that results in formation of an EPF (outer or inner) with a bulk composition ($\delta^{18}O_{o/iEPF}$, $\delta^{13}C_{o/iEPF}$) that may or may not be distinct from $\delta^{18}O_{water}$ and $\delta^{13}C_{eDIC}$, and with DIC species that may or may not be in isotopic equilibrium with each other (reflected in Δ_{47} or Δ_{48}). Finer resolution on some of the fractionating steps could be achieved in a modern context through targeted sampling of inhabited water, body tissues and fluids, and shell carbonate, but tracing these steps is not feasible using fossil shell material.

(2) Shell precipitation

Formation of $CaCO_3$ crystals likely occurs through the accretion of many nanoparticles of ACC (e.g. Weiss *et al.*, 2002; Addadi *et al.*, 2006; Jacob *et al.*, 2011; Gal *et al.*, 2014, 2015; Hovden *et al.*, 2015). The initial ACC lithosome is assembled intracellularly in the mantle epithelium from DIC (Rodríguez-Navarro *et al.*, 2016; Wolf *et al.*, 2016). The

Author Manuscript

lithosome is exocytosed and accretes to the growing mineralization front of the shell (whether the lithosome proceeds to the mineralization front wholesale or dissociates and is reformed within the EPF is the subject of debate; see Wolf *et al.*, 2016). As ACC colloids join to the mineralization front, they are dehydrated into space-filling mesocrystals of calcite or aragonite (Cartwright *et al.*, 2012). The resulting $CaCO_3$ polymorph is determined in some measure by the ACC protostructure and the influence of other additives, notably acidic proteins (e.g. Addadi, Raz & Weiner, 2003; Marin & Luquet, 2004; Marin *et al.*, 2007; Cartwright *et al.*, 2012). For detailed reviews of biomineral formation *via* colloid attachment with an ACC precursor, see Addadi *et al*. (2003), Rodríguez-Navarro *et al.* (2016) and Wolf *et al.* (2016). Shell microstructure and mineralogy are hypothesized to result from the action of proteins, crystal competition, and/or a structured organic matrix (for a relevant review, see Checa, 2018). These physical properties can differ between the OSL and ISL (e.g. Marin & Luquet, 2004; Lécuyer, Reynard & Martineau, 2004; Checa, 2018; Carter & Sato, 2020), which suggests a level of independent regulation that may also give rise to geochemical differentiation.

Temperature-dependent relationships are expected to govern the transfer of the composition of the DIC involved in shell mineralization, represented by EPF, to the solid shell (see Section III). However, it is possible for the isotopic equilibrium state of the internal DIC pool to change during the precipitation process, thus introducing new fractionations to the final $CaCO_3$ in the shell. The narrow thickness of the EPF makes this film of fluid especially susceptible to compounding isotopic fractionations, as lateral mixing within the fluid reservoir should be limited. If $CaCO_3$ precipitation occurs from a DIC pool that is in isotopic equilibrium, Δ_{47} or Δ_{48} would record environmental temperatures regardless of bulk $\delta^{18}O_{EPF}/\delta^{13}C_{EPF.}$ Reconstructed $\delta^{18}O_{EPF}$ could grade from ambient water to the products of metabolic fractionation during the EPF formation phase. However, if precipitation occurs

from a DIC pool not in isotopic equilibrium, neither Δ_{47} nor Δ_{48} would record environmental temperatures and biases in both apparent temperature and $\delta^{18}O_{carb}$ mean that $\delta^{18}O_{EPF}$ and $\delta^{13}C_{EPF}$ cannot be reconstructed.

VI. EXAMPLE APPLICATION: SEYMOUR ISLAND, ANTARCTICA (69–66 Ma)

Below, we identify and interpret the environmental and physiological nature of BioDIFs in Δ_{47}, $\delta^{18}O_{carb}$, and $\delta^{13}C_{carb}$ recorded in well-preserved fossil shells of six extinct bivalve species.

(1) Materials and methods

Fossil shells were collected from the shallowly buried López de Bertodano Formation (69–66 Ma, Seymour Island, Antarctica) (Macellari, 1988). For this study, 117 well-preserved shells were screened for diagenetic alteration using X-ray diffraction (XRD), scanning electron microscopy (SEM), and conservative trace element thresholds [see Petersen, Dutton & Lohmann (2016) for detailed description of methodologies]. A total of 31 shells were excluded from further analysis if trace element concentrations at any of the drill sites exceeded conservative threshold values of 500 ppm for Fe and 200 ppm for Mn (Anderson *et al.*, 1994; Ditchfield, Marshall & Pirrie, 1994; Price *et al.*, 2000). Multiple other lines of evidence (including visible growth bands and preservation of nacre, XRD, cathodoluminescence, and SEM; see Petersen *et al*., 2016) indicated that the remaining shells are exceedingly well preserved. We therefore conclude that the chemical signatures recorded in these shells are primary signals that reflect the composition of the layers at the time of formation and are not diagenetically altered.

Eighty-six shells analysed for their oxygen and carbon isotopic composition passed the diagenetic screening: *Lahillia larseni* (Sharman & Newton 1897) (N = 26), *Dozyia*

Author Manuscript

Author Manuscript

drygalskiana (Wilkens 1910) (N = 13), *Eselaevitrigonia regina* (Wilkens 1910) (N = 19), *Nordenskjoldia nordenskjoldi* Wilkens 1910 (N = 8), *Cucullaea antarctica* Wilkens 1907 (N = 18), and *Cucullaea ellioti* Zinsmeister & Macellari 1988 (N = 2). A subset of those shells (N = 18) were also analysed for their clumped isotope composition: *L. larseni* (N = 9), *N. nordenskjoldi* (N = 3), and *C. antarctica* (N = 6). Geochemical results are discussed below at the genus level for simplicity because the two species of genus *Cucullaea* studied do not exhibit significantly different isotopic behaviour. Full details of assessment of shell mineralogy and microstructure are provided as online Supporting Information in Appendix S1. The included taxa have visually apparent OSL and ISL boundaries originating at the pallial line. The macroscopic boundaries correspond to microstructural boundaries, including the presence of a prismatic pallial myostracum visible in all taxa except for *E. regina* (Fig. S1).

To compare OSL and ISL values and avoid biases related to potential intra-annual variability in isotopic composition of shell carbonate, we sampled the shell at multiple ontogenetic points to derive a multi-annual bulk composition for each layer. Samples of shell material were drilled from the umbo, mid-shell, and within 1 cm of the ventral margin for bulk stable isotope analysis (Fig. 2A). Separate larger samples were drilled adjacent to the original sampling sites at the umbo and ventral margin for clumped isotope analysis (Fig. 2A). Isotopic analysis was performed in the University of Michigan Stable Isotope Laboratory using a Kiel device coupled to a Finnigan MAT253 IRMS (for $\delta^{18}O_{carb}$ and $\delta^{13}C_{carb}$) and a custom-built, manual vacuum line and Thermo MAT253 IRMS (for Δ_{47}). Detailed analytical procedures are provided in Petersen *et al*. (2016) and the full results for bulk stable and clumped isotope measurements are provided in Data file S1.

This data set was initially collected to investigate inter-shell differences, without considering inter-layer differences. As a result, some of the umbo/mid-shell/ventral margin

points exclusively sample a single layer, whereas others combine material from multiple layers. For each distinct sample, the relative proportions of ISL and OSL incorporated in the sampled powder were visually estimated by examining the drill hole and using apparent visual contrasts between layers (e.g. colour; density) as benchmarks. An uncertainty of 10% was assumed for all intermediate percentage estimates.

Pure endmember OSL and ISL compositions were directly measured on 65 of 86 samples. In cases where sampled points combined material from both layers, a linear regression against the visually estimated per cent OSL was used to estimate the isotopic composition of the pure endmember layer that was not directly measured in isolation (see Appendix S2 and Fig. S2). Although clumped isotope values do not mix linearly, we can approximate linear mixing in this case since the size of the inter-layer $\delta^{18}O_{carb}$ and $\delta^{13}C_{carb}$ differences both tend to be less than 2‰, where non-linear mixing effects are negligible (Defliese & Lohmann, 2015). In all cases, we consider the OSL and ISL values of an individual specimen to be 'measurably different' when the observed values are outside of the respective error for the separate layer values. Full details of regressions and uncertainty estimates and treatment of outlier values are provided in Appendix S2.

(2) OSL carbonate records the external environment

The isotopic composition of the OSL across all five genera falls in a limited range (Fig. 3A), in agreement with previous reconstructions of temperature and $\delta^{18}O_{water}$ from Seymour Island in the Maastrichtian (e.g. Dutton *et al.*, 2007; Tobin *et al.*, 2012; Mohr *et al.*, 2020). The mean ± 2SD range in $\delta^{18}O_{carb}$ observed was 0.9 ± 2.8‰ (Fig. 3A). There was no significant difference between OSL $\delta^{18}O$ or Δ_{47} values derived from the different taxa present at each stratigraphic height through the section (Appendix S3, Figs S3 and S4). There was greater variability in OSL $\delta^{13}C_{carb}$ values among genera (Fig. 3A). The lack of obvious

Author Manuscript

Author Manuscript

disequilibrium effects (based on agreement in Δ_{47} within stratigraphic bins) and the small range of $\delta^{18}O_{carb}$ values at each stratigraphic height suggests that the OSLs of all co-occurring taxa precipitated from fluids with similar isotopic compositions, which we interpret to be the shared ambient water. This suggests that the OSLs of all these genera are equally good recorders of shared environmental values, and that BioDIFs are absent. This is consistent with numerous sclerochronology studies, which primarily target the OSL and closely link changes in $\delta^{18}O_{carb}$ to environmental parameters (see review by Moss *et al*., 2021).

(3) Species-specific BioDIFs detected in ISL

Despite close agreement in OSL compositions across taxa, ISL compositions systematically differed from the OSL, and these BioDIFs varied among taxa.

(*a*) *Isotopic trends in ISL values*

Median differences between ISL and OSL $\delta^{18}O_{carb}$ values within individual shells tend to be outside typical analytical error (~0.1‰) for *Lahillia*, *Nordenskjoldia*, and *Cucullaea* (Fig. 3B). For *Dozyia* and *Eselaevitrigonia*, individuals tend to show differences between ISL and OSL $\delta^{18}O$ values that are smaller than the analytical error (see also Fig. S4). Median differences between ISL and OSL $\delta^{13}C_{carb}$ within a single individual was outside analytical error (~0.1‰) for all five genera (Fig. 3B). Median difference between ISL and OSL Δ_{47} within a single individual was outside analytical error (~0.01‰) for *Lahillia* and *Cucullaea* (Fig. 3B), and there was no measurable difference between layers in Δ_{47} for *Norkenskjoldia*. Good agreement in layer averages from different individuals of the same genus and across genera (in the case of the OSL) indicate that the overall OSL and ISL values capture a time-averaged signal, incorporating material from early to late life, and should therefore be reasonably comparable when quantifying BioDIFs. Wherever a measurable ISL–OSL offset was observed, the direction and magnitude of the offset was consistent for each parameter in each taxon

Author Manuscript

through time, suggesting this is not a temporal aliasing (i.e. through the stratigraphic section, 3 Myr; see Appendix S3).

We also do not note any clear relationship between microstructural features of the OSL and ISL and their absolute or relative isotopic values. Taxa that have the same basic microstructure in each shell layer, such as *L. larseni* and *C. antarctica*, which have crossed lamellar aragonite in both shell layers, have large inter-layer isotopic differences that moreover are opposite in relative values between their layers. In the case of *D. drygalskiana*, the same microstructural features have little to no BioDIFs. Other microstructures do not appear to show clear isotopic relationships either. Although there are no emergent trends in this data set, a larger and more diverse suite of taxa would need to be studied to determine with confidence how or whether BioDIFs change with shell microstructure.

(*b*) *Identifying types of BioDIFs*

Because the OSL is inferred to represent palaeoenvironment accurately for all of these taxa, a measurable difference in $\delta^{18}O_{carb}$, $\delta^{13}C_{carb}$ and/or Δ_{47} between the ISL and the OSL indicates a BioDIF affecting the ISL. If Δ_{47} in the ISL differs from Δ_{47} in the OSL, a BioDIF occurred during the precipitation phase such that $\delta^{18}O_{carb}$ and $\delta^{13}C_{carb}$ do not reflect only $\delta^{18}O_{iEPF}$ and $\delta^{13}C_{iEPF}$. Because $\delta^{18}O_{iEPF}$ and $\delta^{13}C_{iEPF}$ cannot be resolved, it is also not possible to determine $\delta^{18}O_{water}$ and $\delta^{13}C_{eDIC}$, so it is ambiguous whether there was or was not a BioDIF introduced during the EPF formation phase. If Δ_{47} in the ISL is equal to Δ_{47} in the OSL, $\delta^{18}O_{carb}$ and $\delta^{13}C_{carb}$ do reflect $\delta^{18}O_{iEPF}$ and $\delta^{13}C_{iEPF}$. In this case, the $\delta^{18}O_{iEPF}$ and $\delta^{13}C_{iEPF}$ calculated for the ISL can be compared to the $\delta^{18}O_{oEPF}$ and $\delta^{13}C_{oEPF}$ (which are theoretically equivalent to $\delta^{18}O_{water}$ and $\delta^{13}C_{eDIC}$) to determine whether a BioDIF occurred during the EPF formation phase.

The results for *Nordenskjoldia* show an EPF formation phase BioDIF and no precipitation phase BioDIF. Similarities in Δ_{47} between ISL and OSL carbonate indicate that ISL carbonate

Author Manuscript

records environmental temperatures and thus both iEPF and oEPF DIC must be in or near isotopic (and chemical) equilibrium. However, remaining depletions in $\delta^{18}O_{carb}$ and $\delta^{13}C_{carb}$ in the ISL relative to OSL indicate the $\delta^{18}O_{iEPF}$ and $\delta^{13}C_{iEPF}$ may be slightly distinct from $\delta^{18}O_{water}$ and $\delta^{13}C_{eDIC}$.

For *Dozyia* and *Eselaevitrigonia* there are small EPF formation phase BioDIFs and likely no precipitation phase BioDIFs. No Δ_{47} data was collected from *Dozyia* or *Eselaevitrigonia* to confirm equilibrium precipitation. However, small enrichments in $\delta^{18}O_{carb}$ and small to moderate enrichments in $\delta^{13}C_{carb}$ in the ISLs of these taxa relative to the OSLs of the same individuals suggest that if precipitation occurred from a fluid in carbonate equilibrium, $\delta^{18}O_{iEPF}$ and $\delta^{13}C_{iEPF}$ may diverge only slightly from $\delta^{18}O_{water}$ and $\delta^{13}C_{eDIC}$.

For *Lahillia* and *Cucullaea* precipitation phase BioDIFs are observed, and it is therefore impossible to determine whether or not there was also an EPF formation phase BioDIF. The ISLs of these two taxa show Δ_{47} values that are different from the OSL, indicating the ISL precipitated out of isotopic equilibrium with iEPF. Because bivalves are ectothermic, there is no physical way that the temperature at the mineralization front could be elevated or reduced from background environmental temperatures by enough to affect isotopic clumping. The Δ_{47} values between layers should therefore always be the same if temperature is the only control on clumping. Different Δ_{47}-based temperature estimates between layers thus indicates isotopic disequilibrium in the iEPF at the time of precipitation (i.e. a precipitation phase BioDIF). Because of disequilibrium skewing Δ_{47}-based temperatures and $\delta^{18}O_{carb}$ values, it is impossible to determine $\delta^{18}O_{iEPF}$ accurately and assess if an EPF formation phase BioDIF occurred in addition to a precipitation phase BioDIF, which would have driven $\delta^{18}O_{iEPF}$ and $\delta^{13}C_{iEPF}$ away from $\delta^{18}O_{water}$ and $\delta^{13}C_{eDIC}$.

(4) Potential drivers of BioDIFs

Cucullaea has lower ISL $\delta^{18}O_{carb}$ and $\delta^{13}C_{carb}$ values and higher Δ_{47} values than OSL values; *Lahillia* has higher ISL $\delta^{18}O_{carb}$ and $\delta^{13}C_{carb}$ values and lower Δ_{47} values (Figs 3B, 4)

Author Manuscript

than OSL values. A small number of points ($N = 3$) for *Nordenskjoldia* suggest lower ISL $\delta^{18}O_{carb}$ and $\delta^{13}C_{carb}$ values with no offset in Δ_{47}, though the exact direction and magnitude of offset in Δ_{47} cannot be statistically determined from so few measurements. Even without considering *Nordenskjoldia*, the opposing directions of BioDIFs apparent in the ISL of *Cucullaea* and *Lahillia* indicate two different mechanisms driving isotopic fractionation in the ISL. Further experiments on modern bivalves are required to link isotopic signals in the shell to causal mechanisms, but it is possible to make early predictions about isotopic responses to certain biological conditions using first principles. Below we hypothesize possible physiological mechanisms that could create the two different BioDIF patterns observed in *Cucullaea* and *Lahillia* to demonstrate how such connections could be made.

(*a*) *Enrichment in Δ_{47} with depletion in $\delta^{18}O$ and $\delta^{13}C$*

In *Cucullaea*, we observed enrichment in Δ_{47} and depletion in $\delta^{13}C$ and $\delta^{18}O$ in the ISL relative to the OSL, which is assumed to have equilibrium values as discussed above (Fig. 4). The hypothetical mechanism that we propose to explain this BioDIF is CO_2 absorption (Fig. 5A). Addition of CO_2 *via* respiration (CO_2 absorption) would drive production of HCO_3^- from CO_2. In solutions with a more basic (higher) pH, the $CO_2 \leftrightarrow HCO_3^-$ conversion will mostly occur through hydroxylation reactions (reaction 1, Section IV). The net kinetic effect of these reactions is lower $\delta^{18}O$ and $\delta^{13}C$ and higher Δ_{47} in the HCO_3^- produced. This net kinetic signature is also directly inherited by the CO_3^{2-} formed through reaction 3 because the isotopic equilibration time between HCO_3^- and CO_3^{2-} is very rapid (seconds; Guo & Zhou, 2019). The $CaCO_3$ formed from this isotopically anomalous HCO_3^- and CO_3^{2-} will reflect this disequilibrium signature. If this process caused the described kinetic signature to be recorded in the solid shell, precipitation must happen faster than the isotopic re-equilibration timescale of minutes to hours between CO_2 and HCO_3^-

(Guo & Zhou, 2019). Similar kinetic fractionations affecting $\delta^{18}O$ and $\delta^{13}C$ are also observed in rapidly precipitated synthetic carbonates (although a fractionation in Δ_{47} is not well established in synthetic experiments) (Watkins *et al.*, 2013, 2014; Watkins & Hunt, 2015; Devriendt, Watkins & McGregor, 2017).

Lifespan estimates for Antarctic *Cucullaea* of 20+ years based on growth banding and isotope sclerochronology (Moss *et al.*, 2017) paint a picture of a slow-growing, fairly long-lived bivalve. The preservation of an isotopic disequilibrium signal in the ISL may instead indicate that shell precipitation in *Cucullaea* occurred in short, rapid bursts of activity that outpace carbonate isotopic equilibration in the EPF and/or exceed the rate of production of new EPF. Controlled experimentation on other modern bivalves (e.g. Wilbur & Saleuddin, 1983) found the rate of iEPF replenishment to be on the scale of minutes to hours, similar to the rate of isotopic equilibration between CO_2 and HCO_3^- (Guo & Zhou, 2019; Guo, 2020). In *Cucullaea*, we would therefore be unable to distinguish whether the isotopic re-equilibration timescale or EPF replenishment timescale would have been the limiting factor preventing erasure of the kinetic signature prior to precipitation. It is also possible that disequilibrium in respired CO_2 entering the EPF would compound this effect.

(*b*) *Depletion in Δ_{47} with enrichment in $\delta^{18}O$ and $\delta^{13}C$*

Lahillia shows depletion in Δ_{47} and enrichment in $\delta^{13}C_{carb}$ and $\delta^{18}O_{carb}$ in the ISL relative to the OSL (Fig. 4). The overarching mechanism that we suggest could produce this BioDIF is CO_2 degassing, which might occur in two stages (Fig. 5B, C) analogous to those proposed for speleothems by Guo & Zhou (2019). The first stage may occur when the valves of the shell are closed, causing respired CO_2 to accumulate internally and lower the pH of the EPF (e.g. Crenshaw, 1972; Schöne & Surge, 2012) (Fig. 5B). Dissolution of the shell in this environment would increase the total concentration of DIC within the EPF during this stage

Author Manuscript

of the process. The second stage may commence when the valves reopen and excess CO_2 quickly degasses from the EPF, prompting an increase in pH and carbonate saturation state (Fig. 5C). These conditions would promote reprecipitation of the shell. Precipitation of $CaCO_3$ promotes production of CO_2 from HCO_3^- with lower $\delta^{18}O$ and $\delta^{13}C$ and higher Δ_{47} values. As this CO_2 of lower bulk stable isotope composition is formed from the initial pool of HCO_3^- in the EPF, the residual pool of HCO_3^- that results would develop higher $\delta^{18}O$ and $\delta^{13}C$ values but, because Δ_{47} values unmix non-linearly (Eiler & Schauble, 2004; Defliese & Lohmann, 2015; Guo & Zhou, 2019), lower Δ_{47}. Consequently, $CaCO_3$ that precipitates from this anomalous HCO_3^- or CO_3^{2-} equilibrated with it would record higher $\delta^{18}O$ and $\delta^{13}C$ and lower Δ_{47}. As above, in order for the described residual-kinetic signature to be recorded in the solid shell, precipitation must happen faster than the isotopic re-equilibration timescale of minutes to hours (Guo & Zhou, 2019). This cycle of valve closure and opening would have to be habitual, and enough carbonate laid down under these conditions in order to be measurable in a bulk sample of shell material.

Microscopic observations of the interior of pristine, modern bivalve shells indicate that shell dissolution can occur *in vivo* as a response to increased partial pressure of CO_2 and may also relate to valve closure (e.g. Jokumsen & Fyhn, 1982; Akberali, Brear & Currey, 1983; Melzner *et al.*, 2011; Schöne & Surge, 2012). *In situ* measurements of EPF by Crenshaw (1972) recorded a coeval drop in pH and increase in Ca^{2+} concentration within 15 min of valve closure. These observations indicate that dissolution of the shell may be a response to homeostatic stress, even at very short time intervals (e.g. Jokumsen & Fyhn, 1982; Akberali *et al.*, 1983; Melzner *et al.*, 2011; Schöne & Surge, 2012). High frequency (e.g. daily) cycles of precipitation and resorption or lengthy periods of valve closure would be difficult to detect in fossil shells because microscopically visible dissolution localized to the interior myostracum would be indistinguishable from minor diagenetic dissolution, but

Author Manuscript

isotopic analysis as described above may evidence these processes occurring habitually in *Lahillia larseni*.

(5) Implications for palaeotemperature reconstructions at Seymour Island

The initial study of Petersen *et al.* (2016) did not consider that sampling at different positions on the shell (umbo *versus* ventral margin) inadvertently captured different layers within the shell (typically pure ISL or OSL, respectively) due to preferential erosion of the OSL near the umbo (Fig. 2B). Those authors observed isotopic differences between shell positions and instead interpreted them as ontogenetic trends, potentially relating to seasonal cessation of shell growth during reproduction. The results we present above refute this hypothesis for intra-shell variability in favour of biologically supported explanations for BioDIFs within the ISL. Furthermore, as the original study measured both ISL and OSL, further palaeoclimate interpretations based on this data set should be limited to only the ventral margin samples that are comprised of the OSL, which we infer above to record palaeoclimate conditions accurately. Supplementary Figure S1b of Petersen *et al.* (2016) shows the inferred temperature profile using only samples from the ventral margin. This profile still shows the main climatic trends described in the original publication: warming in the early Maastrichtian, followed by accelerated warming corresponding to the onset of Deccan volcanism (now termed the Late Maastrichtian Warming Event, LMWE), and possibly another temperature increase near the Cretaceous–Paleogene boundary. The magnitude of the LMWE temperature spike in Antarctica using only the data from the ventral margin is ~9 °C. The temperature profiles from the umbo(ISL)-only and ventral margin(OSL)-only data sets share the same key architecture, which indicates that ISL carbonate still reflects some environmental influence, but with an offset caused by BioDIF.

Author Manuscript

Therefore, by measuring and variably mixing both positions/layers, the overall environmental trends remain observable although the absolute values differ.

VII. A WORKFLOW FOR INTERPRETING BioDIFS

During shell growth, the isotopic composition of surrounding water ($\delta^{18}O_{water}$ and $\delta^{13}C_{eDIC}$) is first converted to EPF ($\delta^{18}O_{EPF}$, $\delta^{13}C_{EPF}$) then preserved in the solid shell ($\delta^{18}O_{carb}$, $\delta^{13}C_{carb}$) that is ultimately analysed in the laboratory for environmental or physiological proxies. The $\delta^{18}O_{carb}$ and $\delta^{13}C_{carb}$ values alone cannot distinguish in which biomineralization phase the BioDIFs appear. However, analysing paired Δ_{47} and $\delta^{18}O_{carb}$ or Δ_{48} values can distinguish BioDIFs derived from the EPF formation phase *versus* the precipitation phase. Below we propose a systematic workflow for deconvoluting the timing of these fractionations in each layer of a fossil shell.

In modern shells, BioDIFs can be identified easily in both OSL and ISL carbonate as differences from expected values given analytically measured growth conditions (temperature, $\delta^{18}O_{water}$, $\delta^{13}C_{eDIC}$). In fossil shells, growth conditions are not known *a priori*, but within-shell comparison between the OSL and ISL can still provide information about the extent to which the isotopic composition of each shell layer is independently regulated. Encouragingly, our results in fossil shells support previous observations that the OSL of bivalve shells is usually a reliable palaeoenvironmental archive (e.g. Schöne & Surge, 2012; Henkes *et al.*, 2013; Caldarescu *et al.*, 2021), even when a BioDIF appears present in the ISL. Therefore, assuming the OSL composition reflects true growth conditions [temperature = water temperature (T_{water}), $\delta^{18}O_{oEPF} = \delta^{18}O_{water}$], differences between the isotopic composition of the OSL and ISL can quantify the absolute offset from environmental parameters within the ISL (i.e. the absolute magnitude of the ISL BioDIF). Even if the primary signal in the OSL was to diverge from surrounding environmental conditions ($\delta^{18}O_{oEPF} \neq \delta^{18}O_{water}$,

Author Manuscript

$\delta^{13}C_{oEPF} \neq \delta^{13}C_{eDIC}$), ISL–OSL offsets would still record meaningful differences in BioDIF magnitude and mechanism between the two shell layers.

The necessary first step is to determine whether shell carbonate precipitated from an EPF in isotopic equilibrium. This can be done either separately for both ISL and OSL using paired Δ_{47} and Δ_{48} analyses or by comparing measured shell values to theoretical and empirically derived equilibrium relationships (e.g. Swart *et al.*, 2021; Fiebig *et al.*, 2021). Alternatively, this can be done by comparing the ISL values to the OSL using Δ_{47} values alone, assuming OSL Δ_{47} accurately represents T_{water}. If Δ_{47} (and Δ_{48}) is inferred to reflect T_{water} accurately (in other words, reflect precipitation from an isotopically and chemically equilibrated EPF), then there should be no precipitation phase BioDIF and $\delta^{18}O_{EPF}$ could be reconstructed from Δ_{47}-derived temperature and $\delta^{18}O_{carb}$ following established mineral–water fractionation behaviour (Kim & O'Neil, 1997; Kim *et al.*, 2007) (Scenario A or C in Fig. 6). If Δ_{47} (and Δ_{48}) do not reflect T_{water}, then a precipitation phase BioDIF is present (Scenario B or D in Fig. 6). Continued advancements in understanding of Δ_{47}–Δ_{48} systematics will improve our interpretation of precipitation phase BioDIFs.

To distinguish between scenarios A and C (Fig. 6), comparison with external information about $\delta^{18}O_{water}$ can reveal whether isotopic fractionations were incurred during the EPF formation phase. Specifically, if $\delta^{18}O_{EPF}$ differs from inferred $\delta^{18}O_{water}$ (as determined from another taxon/proxy known to be free of BioDIFs, from an assemblage-based analysis wherein outlier values are identifiable, or from an internal comparison between ISL and OSL assuming the OSL is free of BioDIFs), this would indicate an EPF formation phase BioDIF in the studied shell layer followed by equilibrium precipitation (Scenario C in Fig. 6). If $\delta^{18}O_{EPF}$ agrees with inferred $\delta^{18}O_{water}$, this would indicate no BioDIFs were present in either the EPF formation or precipitation phase (Scenario A in Fig. 6).

Author Manuscript

Author Manuscript

An EPF formation phase BioDIF may reflect many possible processes where fractionation could have occurred as DIC moved through bodily reservoirs. Interpreting these BioDIFs physiologically as we have done for some precipitation phase BioDIFs requires additional insights from studies on modern taxa where soft parts and fluids can be sampled systematically. Tracing EPF formation phase BioDIFs in fossils will need generalizable theory from such modern analogue studies as soft parts and fluids are rarely, if ever, directly preserved in the fossil record.

Distinguishing between scenarios B (precipitation phase BioDIF only; Fig. 6) and D (precipitation and EPF formation phase BioDIF combined; Fig. 6) is more difficult. If Δ_{47} (and Δ_{48}) do not reflect T_{water}, o/iEPF composition cannot be reconstructed from $\delta^{18}O_{carb}$ and Δ_{47}-derived temperature as described above because both Δ_{47} and $\delta^{18}O_{carb}$ may be skewed from expected values. In these scenarios, it is therefore not possible to say whether the o/iEPF itself was isotopically distinct from inhabited water. However, in some circumstances it still may be possible to reconstruct ambient water temperature based on modeled disequilibrium evolution using paired Δ_{47} and Δ_{48} (see Section III.2; Guo, 2020; Bajnai *et al.*, 2020).

Although it is currently impossible to distinguish between Scenarios B and D (Fig. 6) in fossil shells (it would be possible given direct measurements of EPF in modern shells, although this is technically difficult), further information about the mechanism of precipitation phase BioDIF in a given shell can still be gleaned through paired Δ_{47} and Δ_{48} or $\delta^{18}O_{carb}$. In Section VI.4 we identified two possible geochemical mechanisms (CO_2 absorption and CO_2 degassing) for producing specific BioDIF signatures during the precipitation phase that may indicate something about growth rate, rate/mode of EPF replenishment, and intentional or unintentional EPF acidification and reprecipitation. As

more taxa are studied in this systematic way, additional signatures may be described, giving rise to other mechanistic hypotheses.

VIII. IMPLICATIONS AND FUTURE PROSPECTS

Continuing to investigate how BioDIFs track the biological processes governing shell formation and other aspects of metabolism can add a new dimension to our understanding of life in the geological past. Our observations on the Seymour Island sample set suggest there may be unexpected diversity in mechanisms causing BioDIFs among Bivalvia. Differences in physical shell characteristics among lineages such as size, shape, and microstructure are considered inherited traits with evolutionary significance – geochemical variation between shell layers implying differences in biomineralization strategies among lineages could be considered similarly. In our empirical example, both the direction of the ISL–OSL offset and its magnitude differed most strongly between the two most distantly related taxa, *Lahillia* (an arcoid bivalve) and *Cucullaea* (a cardiid bivalve) (Fig. 3B). If measured systematically across modern and fossil taxa, BioDIFs could be assessed alongside other ecological and life-history traits, adding a new source of information about inter- and intragroup diversity in both recent and in deep time.

Regardless of whether specific fractionating processes can be confidently identified in the fossil record, isotopic distinctiveness of the EPF and the shell indicates that the precipitating environment inside the bivalve remains isolated to some degree from the ambient environment. An organism's capacity to buffer potentially stressful changes in the surrounding environment may relate to the overall resistance of a lineage during periods of environmental change. Tantalizingly, the two taxa from Seymour Island that showed the largest BioDIFs (*Lahillia* and *Cucullaea*), are the only ones of the five genera studied here to survive the end-Cretaceous mass extinction. Similar study is needed across more species and

Author Manuscript

Author Manuscript

more periods of environmental change to determine whether this is a signal or a coincidence, but it is interesting to consider the possibility that BioDIFs may provide access to additional information about the adaptability and resilience of certain taxa in the face of environmental perturbations.

The framework developed here aims to shift the perspective on vital effects recorded in biomineralized shell material from a palaeoenvironmental problem to a palaeophysiological proxy. With the addition of novel analytical techniques such as paired Δ_{47}, Δ_{48}, and $\delta^{18}O_{carb}$ measurements to our toolkit, we are better equipped than ever to illuminate portions of the 'black box' of isotopic vital effects in the fossil record. These BioDIFs in $\delta^{18}O_{carb}$, $\delta^{13}C_{carb}$, and Δ_{47} (and Δ_{48}) can fingerprint aspects of shell formation and thus classify differences in biomineralization among taxa, both today and in deep time. These same geochemical tools can also assess the robustness of palaeoenvironmental inference by providing this additional physiological context. Given the diversity and abundance of bivalves through the Phanerozoic and their participation in all five of the major mass extinctions, analysis of BioDIFs within their shells may reveal previously undetected patterns in adaptability, resilience, and survivorship. These historical insights may help inform how this economically and culturally important class may respond to ongoing and impending environmental changes (e.g. Melzner *et al.*, 2011; Waldbusser *et al.*, 2015; Lee, McGill & Fitzer, 2021).

The geochemistry of fossil shells preserves echoes of interactions between the animal and its environment through the millennia. Here we have presented a broadly applicable framework for systematically identifying BioDIFs using $\delta^{18}O_{carb}$, $\delta^{13}C_{carb}$, and Δ_{47} (and Δ_{48}) in fossil shell material so that they can be interrogated for both their palaeoenvironmental and palaeobiological significance in deep time. As our geochemical toolkit continues to expand alongside our understanding of isotopic fractionations at key stages of the biomineralization

process, carbonate isotope geochemistry has the potential to become an informative palaeophysiological proxy. In this way, BioDIFs can be reimagined as a window into the life and times of ancient and extinct taxa living in environments that may be very different from the modern world.

IX. CONCLUSIONS

(1) Although a hindrance to palaeoenvironmental reconstruction, the biologically driven isotopic fractionations influencing shell geochemistry contain useful information about physiology. Reframing mysterious 'vital effects' as quantifiable BioDIFs sets the stage for more deliberate study of how biology and the environment collectively shape the isotopic composition of the shell.

(2) Clumped isotope measurements are necessary to isolate BioDIFs originating in the precipitation phase. Without a specific control on equilibrium state (which is provided by Δ_{47} plus $\delta^{18}O$ or Δ_{48}), the measured shell composition cannot be used to reconstruct $\delta^{18}O_{EPF}$ or $\delta^{13}C_{EPF}$, and by extension $\delta^{18}O_{water}$ or $\delta^{13}C_{eDIC}$.

(3) Despite historically being considered one of the more reliable biogenic carbonates for palaeoclimatology, bivalves cannot be considered essentially free of BioDIFs. This generalization likely stems from the fact that the OSL, which is formed from an EPF that seems to resemble ambient water more closely than does the ISL and is therefore less likely to show a BioDIF, is usually the only shell layer sampled.

(4) Even when the ISL is influenced by BioDIFs, the OSL can still record an accurate environmental signature. Future studies should target the OSL for the most accurate palaeoenvironmental reconstruction. Analysis of the ISL alongside the OSL should become routine to quantify BioDIFs in as many taxa and time periods as possible.

Author Manuscript

(5) BioDIFs that exist among Bivalvia may be widely variable in direction, magnitude, and affected geochemical quantities. Identifying trends in BioDIFs within class Bivalvia is fertile ground for future work.

(6) Studies on modern taxa can help to refine mechanistic interpretations of BioDIFs. However, BioDIFs do not necessarily have to be explained mechanistically in order to be considered alongside other phylogenetically linked characters such as microstructure, shell morphology, and internal structures. If measured systematically across modern and fossil taxa, BioDIFs may show a phylogenetic signal, adding a potential trait to either integrate into existing phylogenetic hypotheses or analyse with other traits in a comparative framework.

X. ACKNOWLEDGEMENTS

Funding for this work was provided by the Ernest A. Novak Fellowship and Scott Turner Award (awarded to A.N.C.), the Sloan Research Fellowship (awarded to S.V.P.), and the Investment in Science Fund at Woods Hole Oceanographic Institution (awarded to W.G.). We acknowledge the contributions of Andrea Dutton, Kyger Lohmann, and Lora Wingate for collection of bulk stable isotope data from Seymour Island shells and initial interpretations of the data set. Elizabeth Oliphant contributed to collection of clumped isotope data and Ziwei Zhang assisted with estimating OSL and ISL fractions at sampling sites on the shells. Tom Tobin and Rachel Mohr contributed productive discussions in the early stages of this project. We also thank G. Farfan and the Smithsonian National Museum of Natural History Biomineralization Group for discussion. We thank the editor Dr John Welch and two anonymous reviewers for their constructive feedback.

XI. REFERENCES

References identified with an asterisk (*) are used only within the supporting information.

Author Manuscript

Author Manuscript

ADDADI, L., JOESTER, D., NUDELMAN, F. & WEINER, S. (2006). Mollusk shell formation: a source of new concepts for understanding biomineralization processes. *Chemistry* **12**, 980–987.

ADDADI, L., RAZ, S. & WEINER, S. (2003). Taking advantage of disorder: amorphous calcium carbonate and its roles in biomineralization. *Advanced Materials* **15**, 959–970.

AKBERALI, H.B., BREAR, K. & CURREY, J.D. (1983). Mechanical and morphological properties of the shell of *Scrobicularia plana* (Da Costa) under normal and stress conditions. *Journal of Molluscan Studies* **49**, 93–97.

ANDERSON, N.T., KELSON, J.R., KELE, S., DAËRON, M., BONIFACIE, M., HORITA, J., MACKEY, T.J., JOHN, C.M., KLUGE, T., PETSCHNIG, P., JOST, A.B., HUNTINGTON, K.W., BERNASCONI, S.M. & BERGMANN, K.D. (2021). A unified clumped isotope thermometer calibration (0.5–1,100°C) using carbonate-based standardization. *Geophysical Research Letters* **48**, e2020GL092069.

ANDERSON, T.F., POPP, B.N., WILLIAMS, A.C., HO, L.-Z. & HUDSON, J.D. (1994). The stable isotopic records of fossils from the Peterborough Member, Oxford Clay Formation (Jurassic), UK: palaeoenvironmental implications. *Journal of the Geological Society* **151**, 125–138.

BAJNAI, D., GUO, W., SPÖTL, C., COPLEN, T.B., METHNER, K., LÖFFLER, N., KRSNIK, E., GISCHLER, E., HANSEN, M., HENKEL, D., PRICE, G.D., RADDATZ, J., SCHOLZ, D. & FIEBIG, J. (2020). Dual clumped isotope thermometry resolves kinetic biases in carbonate formation temperatures. *Nature Communications* **11**, 1–9.

BERNASCONI, S.M., DAËRON, M., BERGMANN, K.D., BONIFACIE, M., MECKLER, A.N., AFFEK, H.P., ANDERSON, N., BAJNAI, D., BARKAN, E., BEVERLY, E., BLAMART, D., BURGENER, L., CALMELS, D., CHADUTEAU, C., CLOG, M., *ET AL.* (2021). InterCarb: A community effort to improve interlaboratory standardization of the carbonate clumped

Author Manuscript

isotope thermometer using carbonate standards. *Geochemistry, Geophysics, Geosystems* **22**, e2020GC009588.

CALDARESCU, D.E., SADATZKI, H., ANDERSSON, C., SCHÄFER, P., FORTUNATO, H. & MECKLER, A.N. (2021). Clumped isotope thermometry in bivalve shells: a tool for reconstructing seasonal upwelling. *Geochimica et Cosmochimica Acta* **294**, 174–191.

CARRÉ, M., BENTALEB, I., BRUGUIER, O., ORDINOLA, E., BARRETT, N.T. & FONTUGNE, M. (2006). Calcification rate influence on trace element concentrations in aragonitic bivalve shells: Evidences and mechanisms. *Geochimica et Cosmochimica Acta* **70**, 4906–4920.

CARRIKER, M. (1992). Prismatic shell formation in continuously isolated (*Mytilus edulis*) and periodically exposed (*Crassostrea virginica*) extrapallial spaces - explicable by the same concept. *American Malacological Bulletin* **9**, 193–197.

CARTER, J.G. & SATO, K. (2020). Part N, Revised, Volume 1, Chapter 2A: Bivalve shell microstructure and mineralogy: shell microstructure terminology. *Treatise Online* **1**, 1–81.

CARTWRIGHT, J.H.E., CHECA, A.G., GALE, J.D., GEBAUER, D. & SAINZ-DÍAZ, C.I. (2012). Calcium carbonate polyamorphism and its role in biomineralization: how many amorphous calcium carbonates are there? *Angewandte Chemie International Edition* **51**, 11960–11970.

CHECA, A.G. (2018). Physical and biological determinants of the fabrication of molluscan shell microstructures. *Frontiers in Marine Science* **5**, 1–21.

CHECA, A.G., SALAS, C., HARPER, E.M. & BUENO-PÉREZ, J. DE D. (2014). Early stage biomineralization in the periostracum of the 'living fossil' bivalve *Neotrigonia*. *PLOS ONE* **9**, e90033.

Author Manuscript

CLARK, M.S., PECK, L.S., ARIVALAGAN, J., BACKELJAU, T., BERLAND, S., CARDOSO, J.C.R., CAURCEL, C., CHAPELLE, G., DE NOIA, M., DUPONT, S., GHARBI, K., HOFFMAN, J.I., LAST, K.S., MARIE, A., MELZNER, F., *ET AL*. (2020). Deciphering mollusc shell production: the roles of genetic mechanisms through to ecology, aquaculture and biomimetics. *Biological Reviews of the Cambridge Philosophical Society* **95**, 1812–1837.

CRENSHAW, M.A. (1972). The inorganic composition of molluscan extrapallial fluid. *The Biological Bulletin* **143**, 506–512.

CROUCH, N.M.A., EDIE, S.M., COLLINS, K.S., BIELER, R. & JABLONSKI, D. (2021). Calibrating phylogenies assuming bifurcation or budding alters inferred macroevolutionary dynamics in a densely sampled phylogeny of bivalve families. *Proceedings. Biological Sciences* **288**, 20212178.

DAËRON, M., DRYSDALE, R.N., PERAL, M., HUYGHE, D., BLAMART, D., COPLEN, T.B., LARTAUD, F. & ZANCHETTA, G. (2019). Most Earth-surface calcites precipitate out of isotopic equilibrium. *Nature Communications* **10**, 1–7.

DEFLIESE, W.F. & LOHMANN, K.C. (2015). Non-linear mixing effects on mass-47 CO_2 clumped isotope thermometry: patterns and implications. *Rapid Communications in Mass Spectrometry* **29**, 901–909.

DEVRIENDT, L.S., WATKINS, J.M. & MCGREGOR, H.V. (2017). Oxygen isotope fractionation in the $CaCO_3$-DIC-H_2O system. *Geochimica et Cosmochimica Acta* **214**, 115–142.

DITCHFIELD, P.W., MARSHALL, J.D. & PIRRIE, D. (1994). High latitude palaeotemperature variation: new data from the Thithonian to Eocene of James Ross Island, Antarctica. *Palaeogeography, Palaeoclimatology, Palaeoecology* **107**, 79–101.

Author Manuscript

DUTTON, A., HUBER, B.T., LOHMANN, K.C. & ZINSMEISTER, W.J. (2007). High-resolution stable isotope profiles of a dimitobelid belemnite: implications for paleodepth habitat and late maastrichtian climate seasonality. *PALAIOS* **22**, 642–650.

EILER, J.M. (2007). "Clumped-isotope" geochemistry—The study of naturally-occurring, multiply-substituted isotopologues. *Earth and Planetary Science Letters* **262**, 309–327.

EILER, J.M. & SCHAUBLE, E. (2004). $^{18}O^{13}C^{16}O$ in Earth's atmosphere. *Geochimica et Cosmochimica Acta* **68**, 4767–4777.

ELLIOT, M., DEMENOCAL, P.B., LINSLEY, B.K. & HOWE, S.S. (2003). Environmental controls on the stable isotopic composition of *Mercenaria mercenaria*: potential application to paleoenvironmental studies. *Geochemistry, Geophysics, Geosystems* **4**, 1–16.

EPSTEIN, S., BUCHSBAUM, R., LOWENSTAM, H. & UREY, H.C. (1951). Carbonate-water isotopic temperature scale. *GSA Bulletin* **62**, 417–426.

EZARD, T.H.G., EDGAR, K.M. & HULL, P.M. (2015). Environmental and biological controls on size-specific $\delta^{13}C$ and $\delta^{18}O$ in recent planktonic foraminifera. *Paleoceanography* **30**, 151–173.

FENGER, T., SURGE, D., SCHÖNE, B. & MILNER, N. (2007). Sclerochronology and geochemical variation in limpet shells (*Patella vulgata*): a new archive to reconstruct coastal sea surface temperature. *Geochemistry, Geophysics, Geosystems* **8**, 1–17.

FIEBIG, J., DAËRON, M., BERNECKER, M., GUO, W., SCHNEIDER, G., BOCH, R., BERNASCONI, S.M., JAUTZY, J. & DIETZEL, M. (2021). Calibration of the dual clumped isotope thermometer for carbonates. *Geochimica et Cosmochimica Acta* **312**, 235–256.

GAL, A., KAHIL, K., VIDAVSKY, N., DEVOL, R.T., GILBERT, P.U.P.A., FRATZL, P., WEINER, S. & ADDADI, L. (2014). Particle accretion mechanism underlies biological crystal

Author Manuscript

growth from an amorphous precursor phase. *Advanced Functional Materials* **24**, 5420–5426.

GAL, A., WEINER, S. & ADDADI, L. (2015). A perspective on underlying crystal growth mechanisms in biomineralization: solution mediated growth versus nanosphere particle accretion. *CrystEngComm* **17**, 2606–2615.

GANNON, M.E., PÉREZ-HUERTA, A., AHARON, P. & STREET, S.C. (2017). A biomineralization study of the Indo-Pacific giant clam *Tridacna gigas*. *Coral Reefs* **36**, 503–517.

GHOSH, P., ADKINS, J., AFFEK, H., BALTA, B., GUO, W., SCHAUBLE, E.A., SCHRAG, D. & EILER, J.M. (2006). ^{13}C–^{18}O bonds in carbonate minerals: a new kind of paleothermometer. *Geochimica et Cosmochimica Acta* **70**, 1439–1456.

GILLIKIN, D.P., LORRAIN, A., MENG, L. & DEHAIRS, F. (2007). A large metabolic carbon contribution to the $\delta^{13}C$ record in marine aragonitic bivalve shells. *Geochimica et Cosmochimica Acta* **71**, 2936–2946.

GUO, W. (2020). Kinetic clumped isotope fractionation in the DIC-H_2O-CO_2 system: Patterns, controls, and implications. *Geochimica et Cosmochimica Acta* **268**, 230–257.

GUO, W. & ZHOU, C. (2019). Patterns and controls of disequilibrium isotope effects in speleothems: Insights from an isotope-enabled diffusion-reaction model and implications for quantitative thermometry. *Geochimica et Cosmochimica Acta* **267**, 196–226.

HENKES, G.A., PASSEY, B.H., WANAMAKER, A.D., GROSSMAN, E.L., AMBROSE, W.G. & CARROLL, M.L. (2013). Carbonate clumped isotope compositions of modern marine mollusk and brachiopod shells. *Geochimica et Cosmochimica Acta* **106**, 307–325.

Author Manuscript

HOVDEN, R., WOLF, S.E., HOLTZ, M.E., MARIN, F., MULLER, D.A. & ESTROFF, L.A. (2015). Nanoscale assembly processes revealed in the nacroprismatic transition zone of Pinna nobilis mollusc shells. *Nature Communications* **6**, 10097. Nature Publishing Group.

JACOB, D.E., WIRTH, R., SOLDATI, A.L., WEHRMEISTER, U. & SCHREIBER, A. (2011). Amorphous calcium carbonate in the shells of adult *Unionoida*. *Journal of Structural Biology* **173**, 241–249.

JOKUMSEN, A. & FYHN, H.J. (1982). The influence of aerial exposure upon respiratory and osmotic properties of haemolymph from two intertidal mussels, *Mytilus edulis L*. and *Modiolus modiolus L*. *Journal of Experimental Marine Biology and Ecology* **61**, 189–203.

JONES, D.S., WILLIAMS, D.F. & ROMANEK, C.S. (1986). Life history of symbiont-bearing giant clams from stable isotope profiles. *Science* **231**, 46–48.

KELSON, J.R., HUNTINGTON, K.W., SCHAUER, A.J., SAENGER, C. & LECHLER, A.R. (2017). Toward a universal carbonate clumped isotope calibration: Diverse synthesis and preparatory methods suggest a single temperature relationship. *Geochimica et Cosmochimica Acta* **197**, 104–131.

KIM, S.-T. & O'NEIL, J.R. (1997). Equilibrium and nonequilibrium oxygen isotope effects in synthetic carbonates. *Geochimica et Cosmochimica Acta* **61**, 3461–3475.

KIM, S.-T., O'NEIL, J.R., HILLAIRE-MARCEL, C. & MUCCI, A. (2007). Oxygen isotope fractionation between synthetic aragonite and water: Influence of temperature and Mg^{2+} concentration. *Geochimica et Cosmochimica Acta* **71**, 4704–4715.

LÉCUYER, C., REYNARD, B. & MARTINEAU, F. (2004). Stable isotope fractionation between mollusc shells and marine waters from Martinique Island. *Chemical Geology* **213**, 293–305.

Author Manuscript

LEE, T.H., MCGILL, R.A.R. & FITZER, S. (2021). Effects of extra feeding combined with ocean acidification and increased temperature on the carbon isotope values ($\delta^{13}C$) in the mussel shell. *Journal of Experimental Marine Biology and Ecology* **541**, 1–9.

LORRAIN, A., PAULET, Y.-M., CHAUVAUD, L., DUNBAR, R., MUCCIARONE, D. & FONTUGNE, M. (2004). $\delta^{13}C$ variation in scallop shells: increasing metabolic carbon contribution with body size? *Geochimica et Cosmochimica Acta* **68**, 3509–3519.

MACELLARI, C.E. (1988). Stratigraphy, sedimentology, and paleoecology of Upper Cretaceous/Paleocene shelf-deltaic sediments of Seymour Island. In *Geology and Paleontology of Seymour Island Antarctic Peninsula* (eds R.M. FELDMANN & M.O. WOODBURNE), pp. 25–53. Geological Society of America.

MACKENSEN, A. & SCHMIEDL, G. (2019). Stable carbon isotopes in paleoceanography: atmosphere, oceans, and sediments. *Earth-Science Reviews* **197**, 102893.

MARIN, F. & LUQUET, G. (2004). Molluscan shell proteins. *Comptes Rendus Palevol* **3**, 469–492.

MARIN, F., LUQUET, G., MARIE, B. & MEDAKOVIC, D. (2007). Molluscan shell proteins: Primary structure, origin, and evolution. In *Current Topics in Developmental Biology* pp. 209–276. Academic Press.

MCCONNAUGHEY, T. (1989). ^{13}C and ^{18}O isotopic disequilibrium in biological carbonates: I. Patterns. *Geochimica et Cosmochimica Acta* **53**, 151–162.

MCCONNAUGHEY, T.A., BURDETT, J., WHELAN, J.F. & PAULL, C.K. (1997). Carbon isotopes in biological carbonates: respiration and photosynthesis. *Geochimica et Cosmochimica Acta* **61**, 611–622.

MCCONNAUGHEY, T.A. & GILLIKIN, D.P. (2008). Carbon isotopes in mollusk shell carbonates. *Geo-Marine Letters* **28**, 287–299.

Author Manuscript

*McCorkle, D.C., Emerson, S.R. & Quay, P.D. (1985). Stable carbon isotopes in marine porewaters. *Earth and Planetary Science Letters* **74**, 13–26.

Melzner, F., Stange, P., Trübenbach, K., Thomsen, J., Casties, I., Panknin, U., Gorb, S.N. & Gutowska, M.A. (2011). Food supply and seawater pCO_2 impact calcification and internal shell dissolution in the blue mussel *Mytilus edulis*. *PLOS ONE* **6**, e24223.

Mohr, R.C., Tobin, T.S., Petersen, S.V., Dutton, A. & Oliphant, E. (2020). Subannual stable isotope records reveal climate warming and seasonal anoxia associated with two extinction intervals across the Cretaceous-Paleogene boundary on Seymour Island, Antarctica. *Geology* **48**, 1131–1136.

Moss, D.K., Ivany, L.C. & Jones, D.S. (2021). Fossil bivalves and the sclerochronological reawakening. *Paleobiology* **47**, 551–573.

Moss, D.K., Ivany, L.C., Silver, R.B., Schue, J. & Artruc, E.G. (2017). High-latitude settings promote extreme longevity in fossil marine bivalves. *Paleobiology* **43**, 365–382.

Moura, G., Machado, J. & Coimbra, J. (2003). Insights on nacre formation in the freshwater clam *Anodonta cygnea* (*L.*): An overview. In *Biomineralization: Formation, Diversity, Evolution and Application* (eds I. Kobayashi & H. Osawa), pp. 129–132. Tokai University Press, Kanagawa.

Moura, G., Vilarinho, L., Santos, A.C. & Machado, J. (2000). Organic compounds in the extrapalial fluid and haemolymph of *Anodonta cygnea* (*L.*) with emphasis on the seasonal biomineralization process. *Comparative Biochemistry and Physiology. Part B, Biochemistry & Molecular Biology* **125**, 293–306.

Author Manuscript

NAKAHARA, H. (1991). Nacre formation in bivalve and gastropod molluscs. In *Mechanisms and Phylogeny of Mineralization in Biological Systems* (eds S. SUGA & H. NAKAHARA), pp. 343–350. Springer Japan, Tokyo.

NAKAHARA, H. & BEVELANDER, G. (1971). The formation and growth of the prismatic layer of *Pinctada radiata*. *Calcified Tissue Research* **7**, 31–45.

NISHIDA, K. & SASAKI, T. (2018). Geographical and seasonal variations of the shell microstructures in the bivalve *Scapharca broughtonii*. In *Biomineralization* (eds K. ENDO, T. KOGURE & H. NAGASAWA), pp. 177–186. Springer, Singapore.

PARKER, W.G., YANES, Y., SURGE, D. & MESA-HERNÁNDEZ, E. (2017). Calibration of the oxygen isotope ratios of the gastropods *Patella candei crenata* and *Phorcus atratus* as high-resolution paleothermometers from the subtropical eastern Atlantic Ocean. *Palaeogeography, Palaeoclimatology, Palaeoecology* **487**, 251–259.

PETERSEN, S.V., DEFLIESE, W.F., SAENGER, C., DAËRON, M., HUNTINGTON, K.W., JOHN, C.M., KELSON, J.R., BERNASCONI, S.M., COLMAN, A.S., KLUGE, T., OLACK, G.A., SCHAUER, A.J., BAJNAI, D., BONIFACIE, M., BREITENBACH, S.F.M., *ET AL.* (2019). Effects of improved ^{17}O correction on interlaboratory agreement in clumped isotope calibrations, estimates of mineral-specific offsets, and temperature dependence of acid digestion fractionation. *Geochemistry, Geophysics, Geosystems* **20**, 3495–3519.

PETERSEN, S.V., DUTTON, A. & LOHMANN, K.C. (2016). End-Cretaceous extinction in Antarctica linked to both Deccan volcanism and meteorite impact via climate change. *Nature Communications* **7**, 1–9.

PONDER, W.F., LINDBERG, D.R. & PONDER, J.M. (2020). The Bivalvia. In *Biology and Evolution of the Mollusca* pp. 109–181, 1st edition. CRC Press, Boca Raton, FL.

Author Manuscript

PRICE, G.D., RUFFELL, A.H., JONES, C.E., KALIN, R.M. & MUTTERLOSE, J. (2000). Isotopic evidence for temperature variation during the early Cretaceous (late Ryazanian–mid-Hauterivian). *Journal of the Geological Society* **157**, 335–343.

RODRÍGUEZ-NAVARRO, C., RUIZ-AGUDO, E., HARRIS, J. & WOLF, S.E. (2016). Nonclassical crystallization in vivo et in vitro (II): Nanogranular features in biomimetic minerals disclose a general colloid-mediated crystal growth mechanism. *Journal of Structural Biology* **196**, 260–287.

ROMANEK, C.S., JONES, D.S., WILLIAMS, D.F., KRANTZ, D.E. & RADTKE, R. (1987). Stable isotopic investigation of physiological and environmental changes recorded in shell carbonate from the giant clam *Tridacna maxima*. *Marine Biology* **94**, 385–393.

SCHÖNE, B. & SURGE, D. (2012). no. 46: Part N, Revised, Volume 1, Chapter 14: Bivalve sclerochronology and geochemistry. *Treatise Online* **46**, 1–24.

SCHÖNE, B.R. (2008). The curse of physiology—challenges and opportunities in the interpretation of geochemical data from mollusk shells. *Geo-Marine Letters* **28**, 269–285.

SHANAHAN, T.M., PIGATI, J.S., DETTMAN, D.L. & QUADE, J. (2005). Isotopic variability in the aragonite shells of freshwater gastropods living in springs with nearly constant temperature and isotopic composition. *Geochimica et Cosmochimica Acta* **69**, 3949–3966.

SWART, P.K., LU, C., MOORE, E.W., SMITH, M.E., MURRAY, S.T. & STAUDIGEL, P.T. (2021). A calibration equation between Δ_{48} values of carbonate and temperature. *Rapid Communications in Mass Spectrometry* **35**, e9147.

TOBIN, T.S., WARD, P.D., STEIG, E.J., OLIVERO, E.B., HILBURN, I.A., MITCHELL, R.N., DIAMOND, M.R., RAUB, T.D. & KIRSCHVINK, J.L. (2012). Extinction patterns, $\delta^{18}O$ trends, and magnetostratigraphy from a southern high-latitude Cretaceous–Paleogene

Author Manuscript

section: Links with Deccan volcanism. *Palaeogeography, Palaeoclimatology, Palaeoecology* **350–352**, 180–188.

WALDBUSSER, G.G., HALES, B., LANGDON, C.J., HALEY, B.A., SCHRADER, P., BRUNNER, E.L., GRAY, M.W., MILLER, C.A., GIMENEZ, I. & HUTCHINSON, G. (2015). Ocean acidification has multiple modes of action on bivalve larvae. *PLOS ONE* **10**, e0128376.

WATKINS, J.M. & HUNT, J.D. (2015). A process-based model for non-equilibrium clumped isotope effects in carbonates. *Earth and Planetary Science Letters* **432**, 152–165.

WATKINS, J.M., HUNT, J.D., RYERSON, F.J. & DEPAOLO, D.J. (2014). The influence of temperature, pH, and growth rate on the $\delta^{18}O$ composition of inorganically precipitated calcite. *Earth and Planetary Science Letters* **404**, 332–343.

WATKINS, J.M., NIELSEN, L.C., RYERSON, F.J. & DEPAOLO, D.J. (2013). The influence of kinetics on the oxygen isotope composition of calcium carbonate. *Earth and Planetary Science Letters* **375**, 349–360.

WEINER, S. & DOVE, P.M. (2003). An overview of biomineralization processes and the problem of the vital effect. *Reviews in Mineralogy and Geochemistry* **54**, 1–29.

WEISS, I.M., TUROSS, N., ADDADI, L. & WEINER, S. (2002). Mollusc larval shell formation: amorphous calcium carbonate is a precursor phase for aragonite. *Journal of Experimental Zoology* **293**, 478–491.

WILBUR, K.M. & SALEUDDIN, A.S.M. (1983). 6 - Shell Formation. In *The Mollusca* (eds A.S.M. SALEUDDIN & K.M. WILBUR), pp. 235–287. Academic Press.

WOLF, S.E., BÖHM, C.F., HARRIS, J., DEMMERT, B., JACOB, D.E., MONDESHKI, M., RUIZ-AGUDO, E. & RODRÍGUEZ-NAVARRO, C. (2016). Nonclassical crystallization in vivo et in vitro (I): Process-structure-property relationships of nanogranular biominerals. *Journal of Structural Biology* **196**, 244–259.

YARRA, T., BLAXTER, M. & CLARK, M.S. (2021). A bivalve biomineralization toolbox. *Molecular Biology and Evolution* **38**, 4043–4055.

ZHOU, G.-T. & ZHENG, Y.F. (2006). On the direction and magnitude of oxygen isotope fractionation between calcite and aragonite at thermodynamic equilibrium. *Aquatic Geochemistry* **12**, 239–268.

* ZINSMEISTER, W.J. (2001). Late Maastrichtian short-term biotic events on Seymour Island, Antarctic Peninsula. *The Journal of Geology* **109**, 213–229.

XII. SUPPORTING INFORMATION

Additional supporting information may be found online in the Supporting Information section at the end of the article.

Appendix S1. Shell mineralogy and microstructure

Fig. S1. Microstructure of outer shell layer (OSL), inner shell layer (ISL), and the inter-layer boundary.

Data file S1. (See separate Excel file). Sample information and isotopic results.

Appendix S2. Regression of endmember values from mixed-layer samples, error propagation, and discussion of outlier values.

Fig. S2. Example of error propagation through the linear regression step.

Appendix S3. Geochemical variability through time.

Fig. S3. Stratigraphic occurrences of study taxa.

Fig. S4. Detailed geochemical results from Seymour Island taxa.

Author Manuscript

Author Manuscript

Figure legends

Fig. 1. Schematic diagram of bivalve anatomy and pathways for transformation of water into shell material. Arrow 1: extrapallial fluid (EPF) formation phase; 1a: uptake of external dissolved inorganic carbonate (eDIC) from ambient water by the mantle/possible mixing with outer extrapallial fluid (oEPF); 1b: transport of eDIC and metabolic dissolved inorganic carbonate (mDIC) to the EPF *via* the mantle and visceral mass. Arrow 2: precipitation phase. The thickness of the extrapallial space and the mantle epithelium is exaggerated for clarity. iEPF, inner extrapallial fluid; ISL, inner shell layer; OSL, outer shell layer.

Fig. 2. Locations of sample collection from shells. (A) Example drill paths for bulk stable and clumped isotopes. Each shell was drilled either in cross sectional view (black circles) or inwards from the exterior (green boxes) near the umbo, mid-shell, and ventral margin for bulk stable isotopes and a subset of shells were also drilled for clumped isotopes. The shorter exterior bulk stable isotope drill paths represent samples of only the outer shell layer (OSL). The longer exterior bulk stable isotope drill paths represent samples of mixed OSL and inner shell layer (ISL), where layer composition had to be resolved by linear regression (see Fig. S1). (B) Umbo of *C. antarctica* specimen C1184A showing complete erosion of the OSL. Note that the OSL was drilled at the mid-shell, but only the ISL sampled at the eroded umbo.

Fig. 3. Geochemical results from Maastrichtian age bivalves of Seymour Island, Antarctica. (A) Paired outer shell layer (OSL) and inner shell layer (ISL) values for each taxon. Number of samples (*N*) is indicated above box and whisker plot in grey. (B) Magnitude and direction of offset from the OSL to the ISL in all individuals where both values were measured/calculated for each taxon. Positive values indicate the ISL had a higher value than the OSL and *vice versa*. Dashed line at 0‰ indicates no difference between layers. Thick

Author Manuscript

black line within boxes indicates median value. Box extends from first quartile to third quartile. Whiskers extend to the minimum and maximum values that are within 1.5 times the interquartile range on either side. Individual points are measurements falling outside the maximum or minimum thresholds. Median ISL–OSL difference indicated above each box and whisker plot. Number of samples (*N*) indicated above box and whisker plot in grey. The $\delta^{18}O$ and $\delta^{13}C$ values are reported relative to the Vienna Peedee Belemnite standard. Skull and crossbones next to genus indicates that the taxon disappeared in the section prior to the Cretaceous–Paleogene mass extinction. Phylogenetic relationships among genera in B are from Crouch *et al*. (2021).

Fig. 4. Disequilibrium plots for (A) Δ_{47} *versus* $\delta^{18}O_{carb}$ and (B) Δ_{47} *versus* $\delta^{13}C_{carb}$. The outer shell layer (OSL) is used as the environmental reference point for each shell, which circumvents the need to assume a specific $\delta^{18}O_{water}$ value in these plots. $\delta^{18}O$ and $\delta^{13}C$ values are reported relative to the Vienna Peedee Belemnite standard. Error bars show propagated uncertainty calculated as described in Appendix S2.

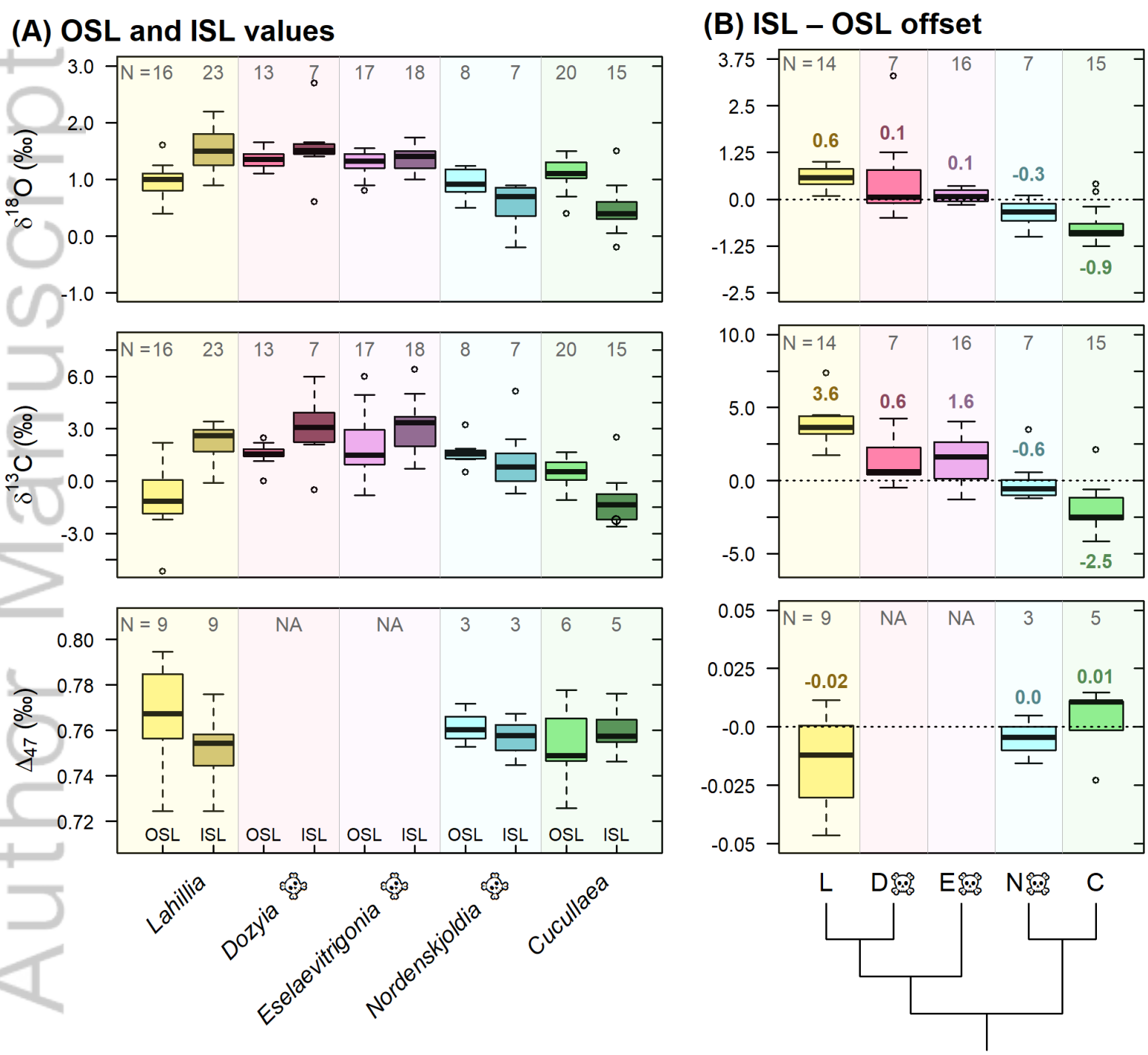
Fig. 5. Hypothesized mechanisms for the observed disequilibrium effects in the dissolved inorganic carbonate (DIC) pool used in bivalve shell formation. Pictorial representations of chemical reactions show the predominant pathway generating the kinetic signature recorded in the shell as a sequence of unidirectional reactions for simplicity. Note that all reactions are reversible, as written to the right of each panel. Chemical species are coloured according to their kinetic signature (or lack thereof) and the arrows representing the reactions causing the initial fractionation are also coloured accordingly. No kinetic signature is indicated during conversion between CO_3^{2-} and HCO_3^- because of their rapid isotopic equilibration; CO_3^{2-} accordingly is depicted with the same kinetic signature (or lack thereof) as HCO_3^-. Note that

Author Manuscript

the precipitation of $CaCO_3$ is depicted with a single arrow for simplicity, but the formation of space-filling $CaCO_3$ crystals is a multi-step process that is also directed by the mantle epithelium and its secretory products. See Sections II and V for further explanation. (A) Process of CO_2 absorption, which leads to a shell with lower $\delta^{18}O_{carb}$, $\delta^{13}C_{carb}$, and Δ_{48} values but higher Δ_{47} values compared to the equilibrium scenario. (B) Stage I of CO_2 degassing, which may be initiated by accumulation of respired CO_2 during valve closure and result in higher concentrations of DIC within the EPF *via* shell dissolution. (C) Stage II of CO_2 degassing, which may be driven by an increase in pH and carbonate saturation state during shell opening as CO_2 degasses. Precipitation of $CaCO_3$ leads to a reprecipitated shell with higher $\delta^{18}O_{carb}$, $\delta^{13}C_{carb}$, and Δ_{48} values but lower Δ_{47} values compared to the equilibrium scenario. Numbering of reaction steps continues from B. EPF, extrapallial fluid; ME, mantle epithelium; VM, ventral margin.

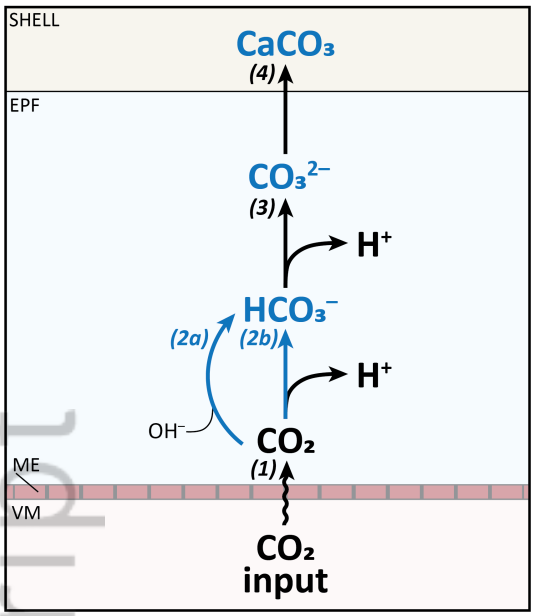
Fig. 6. Possible pathways for biologically driven isotopic fractionation (BioDIF) in bivalves. Grey flowchart (left) depicts the development of BioDIF in the order it would occur during biomineralization *in vivo*. To reconstruct extrapallial fluid (EPF) and inhabited water composition, this order must be reversed beginning with shell composition. Three types of BioDIF resulting from these pathways and the option for no BioDIF are identified with letters A–D (middle). Distinct isotopic composition among reservoirs is represented pictorially by differences in colour for water, EPF, and the shell (pale grey represents the physical boundaries between inhabited water and the EPF). The rightmost panels outline the quantitative palaeoenvironmental information that can be derived from the isotopic composition of the shell layer under each of the four BioDIF scenarios. This workflow can be followed independently for each layer of the shell.

Author Manuscript



BRV_12940_Curley Fig 3.png

(A) CO_2 absorption



4) Formation of $CaCO_3$
$CO_3^{2-} + Ca^{2+} \leftrightarrow CaCO_3$

3) Formation of CO_3^{2-}
$HCO_3^- \leftrightarrow CO_3^{2-} + H^+$

2) Formation of HCO_3^-
a) $CO_2 + OH^- \leftrightarrow HCO_3^-$
b) $CO_2 + H_2O \leftrightarrow HCO_3^- + H^+$

1) Input of CO_2

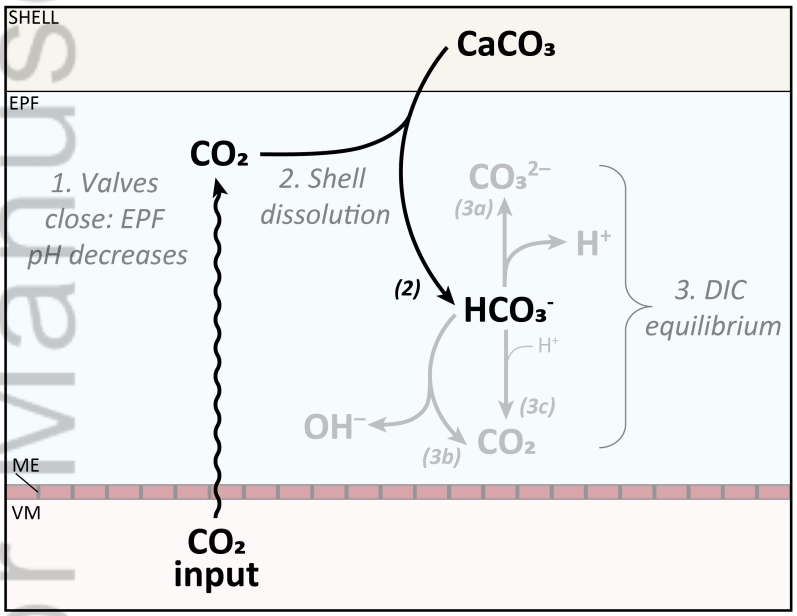
BioDIF

no kinetic signature

kinetic signature
$\downarrow\delta^{18}O$ $\downarrow\delta^{13}C$
$\uparrow\Delta_{47}$ $\downarrow\Delta_{48}$

kinetic signature
$\uparrow\delta^{18}O$ $\uparrow\delta^{13}C$
$\downarrow\Delta_{47}$ $\uparrow\Delta_{48}$

(B) CO_2 degassing: Stage I
(Valves closed) Shell dissolution

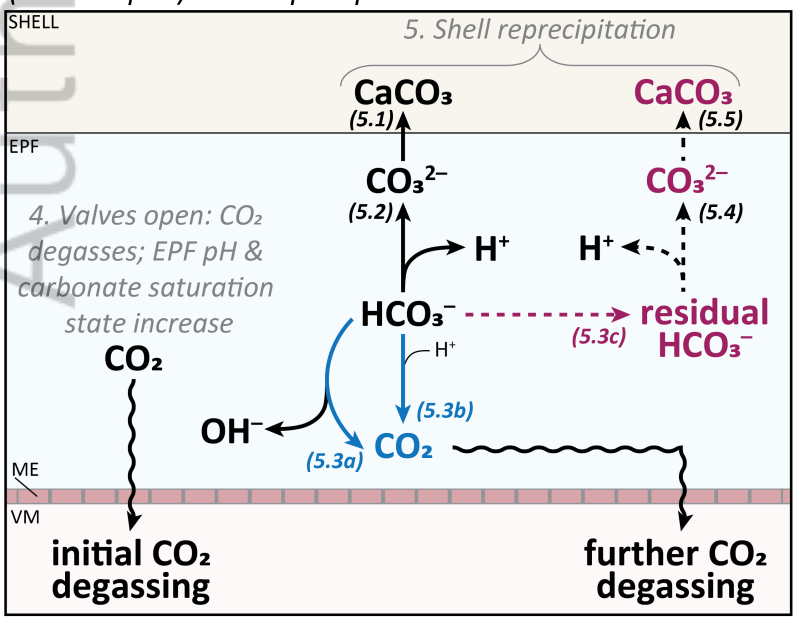


1) Valves close
respired CO_2 accumulates and pH decreases

2) Shell dissolution
$CaCO_3 + H_2O + CO_2 \leftrightarrow 2HCO_3^- + Ca^{2+}$
concentration of DIC increases
(dominated by HCO_3^-)

3) DIC equilibrium
a) $HCO_3^- \leftrightarrow CO_3^{2-} + H^+$
b) $HCO_3^- \leftrightarrow CO_2 + OH^-$
c) $HCO_3^- + H^+ \leftrightarrow CO_2 + H_2O$

(C) CO_2 degassing: Stage II
(Valves open) Shell reprecipitation



4) Valves open
CO_2 degasses leading to pH & carbonate saturation state increase

5) Shell reprecipitation
5.1) Formation of $CaCO_3$
$CO_3^{2-} + Ca^{2+} \leftrightarrow CaCO_3$

5.2) Formation of CO_3^{2-}
$HCO_3^- \leftrightarrow CO_3^{2-} + H^+$

5.3) Formation of CO_2 & residual HCO_3^-
a) $HCO_3^- \leftrightarrow CO_2 + OH^-$ *
b) $HCO_3^- + H^+ \leftrightarrow CO_2 + H_2O$ *
c) formation of residual HCO_3^- by unmixing

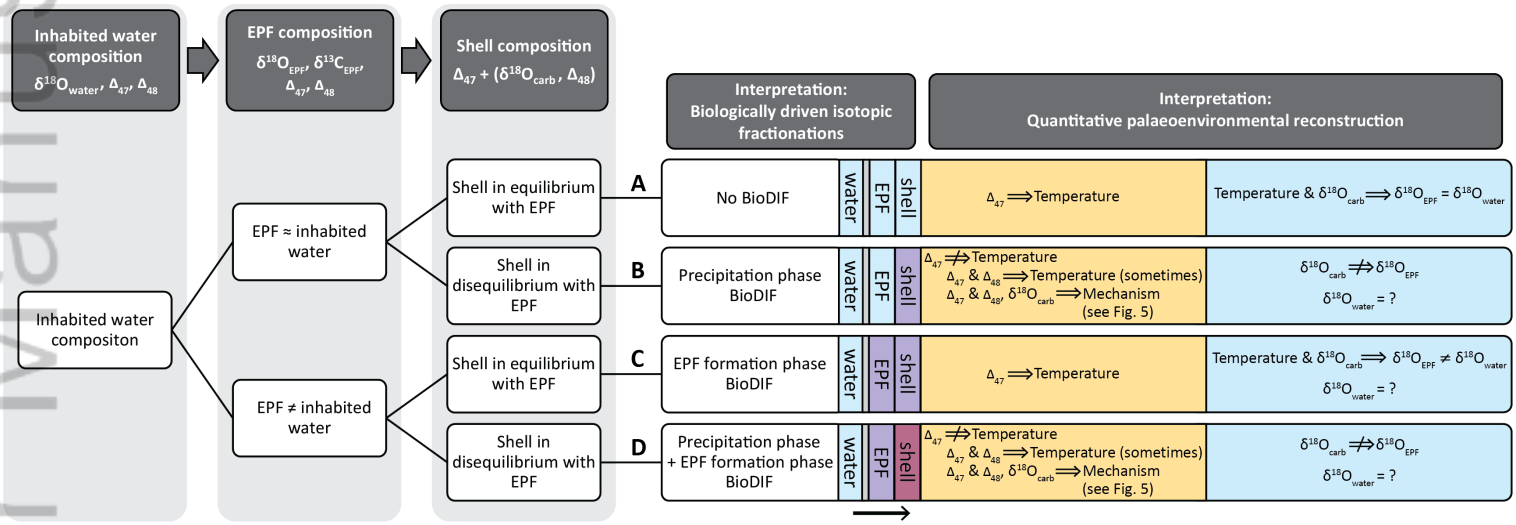
5.4-5.5) Reprecipitation from residual HCO_3^-
same as 5.1–5.2; results in kinetic signature recorded in reprecipitated shell

**excess of produced CO_2 degasses*

Author Manuscript

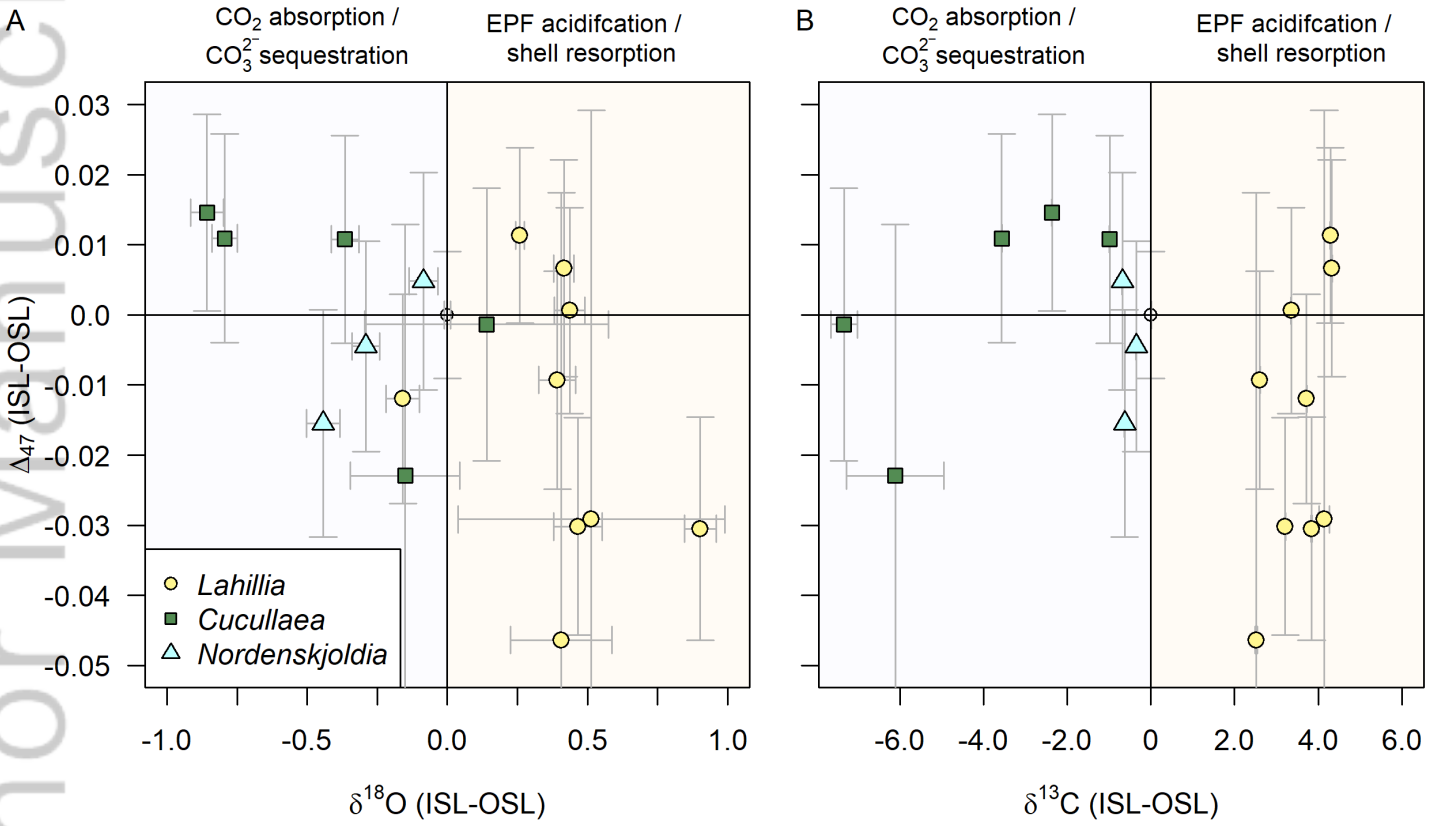
BRV_12940_Curley Fig 5.png

Author Manuscript



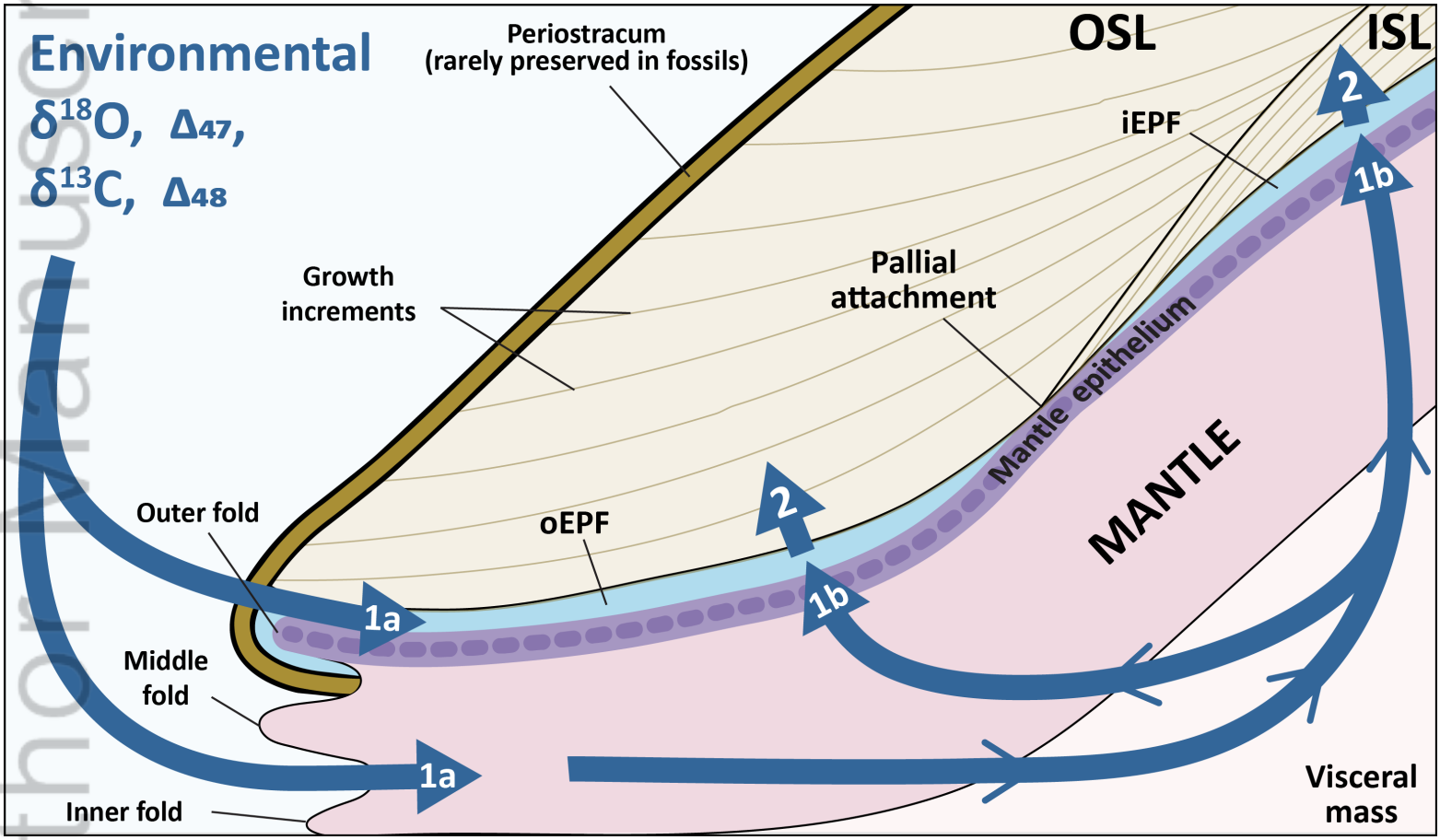
BRV_12940_Curley Fig 6.png

Author Manuscript



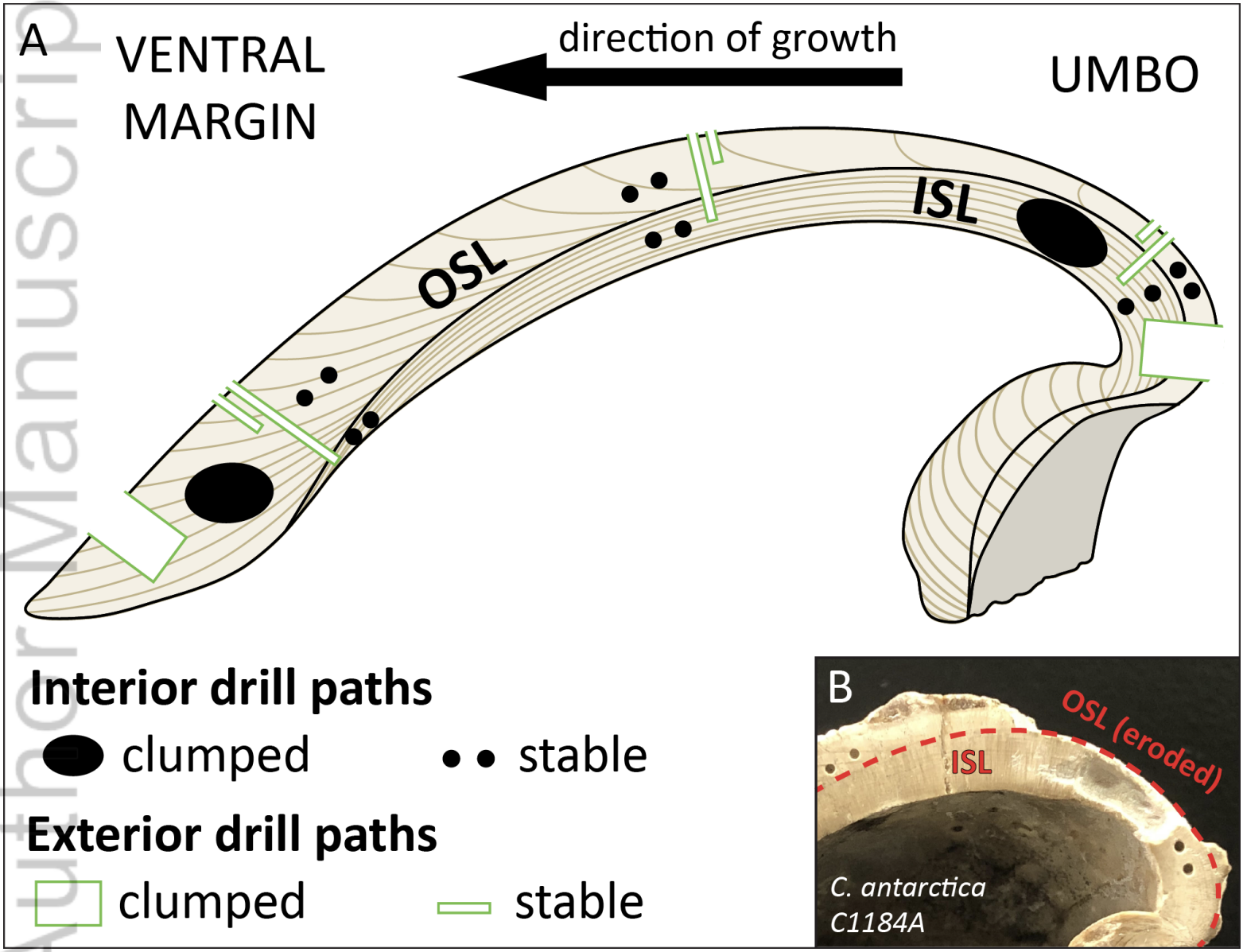
BRV_12940_Curley_Fig4_Revised_ANC_2.png

Author Manuscript



BRV_12940_Curley_Fig 1.png

Author Manuscript



BRV_12940_Curley_Fig 2.png